Journal of Scientific Computing
https://doi.org/10.1007/s10915-018-0861-0

An Asymptotics-Based Adaptive Finite Element Method for Kohn–Sham Equation

Yedan Shen[1] · **Yang Kuang**[1] · **Guanghui Hu**[1,2]

Received: 16 January 2018 / Revised: 16 August 2018 / Accepted: 20 October 2018

Abstract
In Radovitzky and Ortiz (Comput Methods Appl Mech Eng 172(1–4):203–240, 1999), an error estimation technique for nonlinear PDEs is presented to adaptively generating mesh, based on the reduction of the order of the approximate polynomial. In this paper, following a similar analysis framework, we propose an *a posteriori* error estimation for Kohn–Sham equation by coarsening mesh. An upper bound for the difference of the total energies on two successively refined meshes is derived by the numerical solutions on two meshes through an asymptotic analysis, which finally generates an *a posteriori* error estimation. A variety of numerical tests show that such an *a posteriori* error estimation works very well in our h-adaptive finite element method framework. In addition, to further improve the efficiency, we solve a Poisson equation instead of the Kohn–Sham equation on the coarsened mesh. The effectiveness of this improvement is analyzed and numerically examined.

Keywords Electronic structure calculation · Kohn–Sham density functional theory · Adaptive finite element method · Ground state energy · Coarsening mesh

1 Introduction

Kohn–Sham model is one of the most widely used models in the computational quantum chemistry etc. for many-body electronic structure calculations [17,42]. The time-independent Kohn–Sham model takes the form

The authors would like to thank the support from FDCT 029/2016/A1 of Macao S.A.R., MYRG2017-00189-FST from University of Macau, and and National Natural Science Foundation of China (Grant No. 11401608).

✉ Guanghui Hu
garyhu@umac.mo

Yedan Shen
trina1990s@gmail.com

Yang Kuang
kuangyoung0107@gmail.com

[1] Department of Mathematics, University of Macau, Macau, Macao SAR, China

[2] Zhuhai UM Science and Technology Research Institute, Zhuhai, China

Published online: 27 October 2018

$$H\psi_i(\mathbf{r}) = \epsilon_i \psi_i(\mathbf{r}), \quad i = 1, 2, \ldots, N, \tag{1}$$

where H stands for the Hamiltonian operator of the quantum system, N is the number of electrons, and ϵ_i and ψ_i represent the i-th eigenenergy and wavefunction, respectively.

There are two predominant numerical methods for solving the Kohn–Sham equation, i.e., the plane-wave (PW) expansion methods and the real-space methods. The plane-wave expansion methods have attracted considerable attention and widely used in the computational chemistry community [28,40]. One of the main reasons for the popularity of the PW methods is that simple basis set can be quite effective with the help of pseudopotential, especially for the periodic systems. However, for non-periodic boundary conditions and/or domain with complicated geometry, the PW method is not flexible enough. As a result, the real-space methods have been attracting more and more attention, such as the finite difference methods [11,12], the finite element methods [6,35,37], and the discontinuous Galerkin methods [32,42]. Another important issue on numerically solving Kohn–Sham equation is efficiency, especially when the system size is large. Since the existence of the singularity in the external potential term, it can be imagined that a large amount of mesh grids are needed for the quality numerical solutions. To balance the computational resource and the numerical accuracy, a discretization of Kohn–Sham equation on a nonuniform mesh becomes a feasible way. The motivation is straightforward, i.e., by using dense mesh grids in the region with large variation of the numerical solution, while keeping the mesh grids coarse elsewhere, the total amount of the mesh grids can be controlled effectively, and the numerical solution with desired accuracy can be expected. Towards this direction, there are several questions such as how to generate quality nonuniform mesh, and how to efficiently solve the derived linear system. Fortunately, quality answers can be found from the research of adaptive mesh methods.

The adaptive mesh techniques mainly include the r-adaptive methods [7,31,39,43] which redistribute the grid points while keeping the total number of mesh grids unchanged, and h-adaptive methods [6,10,13] which locally refine and coarsen the mesh, and p-adaptive methods [3,23] which locally enrich the order of the basis functions. Particularly, for the application of these adaptive methods in the electronic structure calculations, people may refer to [18,19] for the adaptive coordinates methods, [6,8,13] for the h-adaptive methods, and [7,29] for the r-adaptive methods. When combining with the finite element framework, there are various works devoted to *a posteriori* error estimates [2,5,9,13,16,20,27,30,38]. It is worth mentioning that in [34], the authors proposed a mesh adaption scheme based on an element size distribution function $h(r)$ to minimize the error of the Kohn–Sham problem with a fixed number of elements in the mesh.

The mesh adaption skill presented in the paper [34] is based on the idea of R. Radovitzky et al. [36] in which *a posteriori* error estimation was illustrated for strongly nonlinear dynamics problems. They came up with *a posteriori* error estimation to a static model which is obtained by discretizing the initial boundary value problem in time and making it obey a minimum principle under some conditions. They estimated the error asymptotically between the finite element solution and a lower-order projection of the solution, as $h \to 0$. Then the optimal mesh size distribution function $h(r)$ followed from the *a posteriori* error indicator was adopted to generate a better mesh. In [6], an h-adaptive finite element framework is proposed to solve Kohn–Sham equation, in which the local refinement and coarsening of the mesh grids are handled flexibly and efficiently by using a *Hierarchy Geometry Tree* (HGT) data structure. With HGT and an efficient interpolation between two meshes, the numerical study of the relation between solutions on different meshes becomes very convenient. In this paper, by taking the advantage of HGT, we follow a similar framework in [36] to generate an

a posteriori error estimation by coarsening the mesh for our h-adaptive method. The mesh adaption process is implemented in a similar way to [6]. Moreover, it is noted that the total ground state energy is the target in solving the Kohn–Sham equation, we would derive an error indicator for the total ground state energy directly. As a result, an *a posteriori* error estimation generated from two numerical solutions on different mesh towards the total ground state energy is proposed in this paper.

Based on the *a posteriori* error estimation, an h-adaptive finite element scheme is thus presented for solving the Kohn–Sham equation in this paper. The scheme consists of two parts. The first one is the solution part, i.e., the widely used self-consistent field (SCF) iteration. In this paper, only the all-electron calculation for quantum systems is considered, and both linear and quadratic finite element discretizations will be studied for the Kohn–Sham equation. The Libxc [33] is utilized for generating the exchange-correlation potentials. To obtain the Hartree potential, the associated Poisson equation is solved by using the highly efficient algebraic multigrid method. To solve the generalized eigenvalue problem, the locally optimal block preconditioned conjugate gradient (LOBPCG) method [24,25] is employed. The second part in our algorithm is the mesh adaption part. In this part, the error indicator plays a significant role. Regions in the domain are locally refined or coarsened based on the error indicator that marked on. Precisely, there exist two meshes when implementing the algorithm, i.e., the current mesh $\mathcal{T}^h$ and the coarsened mesh $\mathcal{T}^H$, which is obtained through globally coarsening $\mathcal{T}^h$ for once. By interpolation and projection, information of solution is communicated between $\mathcal{T}^h$ and $\mathcal{T}^H$, and then the error indicator on $\mathcal{T}^H$ following our *a posteriori* error estimation is generated. However, in simulations this error indicator will not be used to guide the mesh adaption for the coarsened mesh $\mathcal{T}^H$, Instead, we use it to refine the current mesh $\mathcal{T}^h$. We do this based on the following considerations. First of all, the error indicators can describe the shape of the error on $\mathcal{T}^H$, and this also holds for $\mathcal{T}^h$ if the numerical solutions on $\mathcal{T}^H$ are in the asymptotic region of the real solutions. Secondly, if we use the indicators to guide the mesh adaption of $\mathcal{T}^H$, it will result in inefficiency of the algorithm, since most of the computational sources are occupied by the implementations on the fine meshes. Meanwhile, the more accurate results on $\mathcal{T}^h$ only contribute to the evaluation of the error indicator, which certainly cause a waste of the computational sources. Therefore, to improve the efficiency of algorithm and make full use of the implementations, the error indicator will be interpolated to the current mesh $\mathcal{T}^h$ so as to guide the mesh adaption on $\mathcal{T}^h$. The numerical results show that our h-adaptive method based on the proposed *a posteriori* error estimation works well in all the simulations. It is noted that on the coarse mesh, a sufficiently accurate Kohn-Sham solution is needed to deliver a quality error estimation. Due to its nonlinearity, it could be time-consuming to solve Kohn-Sham equation on the coarse mesh, even with a good initial condition. To further improve the efficiency, we follow the idea in [21] to replace the Kohn-Sham problem by a Poisson problem on the coarse mesh. Then the solution for this Poisson problem would be used to generate the error estimation. The effectiveness of this improvement is analyzed and numerically tested in detail in Sect. 5.3.

The remainder of the paper is organized as follows. In Sect. 2, the Kohn–Sham density functional theory (DFT) eigenvalue problem is introduced and discretized by finite element method. In Sect. 3, we present the *a posteriori* error estimate for energy based on the numerical solutions from two successively refined meshes. Then the framework of our adaptive finite method is demonstrated in Sect. 4 and the numerical experiments are displayed in Sect. 5. In the end of Sect. 5, a potential improvement of our method is discussed. Finally, the conclusion and future work part are given in the last section.

2 Kohn–Sham Equation and Finite Element Discretization

In this section, we consider a molecular system in $\mathcal{R}^3$ consisting of M nuclei of charges $\{Z_1, \ldots Z_M\}$ located at the positions $\{\mathcal{R}_1, \ldots \mathcal{R}_M\}$ and N electrons in the non-relativistic and spin-unpolarized setting. The ground state solutions of the system can be obtained by solving the lowest N eigenpairs of the following Kohn–Sham equation

$$\begin{cases} H\psi_i = \epsilon_i \psi_i, \quad in \quad \Omega, i = 1, 2, \ldots, N, \\ \int_\Omega \psi_i \psi_j = \delta_{ij}, \quad i, j = 1, 2, \ldots, N, \end{cases} \tag{2}$$

where δ_{ij} is the Kronecker operator. The Hamiltonian H consists of two parts, the kinetic potential part $-\nabla^2/2$ and the effective potential part $V_{eff}([\rho]; \mathbf{r})$ which is given as follows

$$V_{eff} = V_{ext}(\mathbf{r}) + V_{Hartree}([\rho]; \mathbf{r}) + V_{xc}([\rho]; \mathbf{r}), \tag{3}$$

where ρ is the electronic density which can be written as

$$\rho(\mathbf{r}) = \sum_{i=1}^{N} |\psi_i(\mathbf{r})|^2. \tag{4}$$

The first term of the effective potential is the electrostatic potential due to the nuclei which takes the following form

$$V_{ext}(\mathbf{r}) = -\sum_{k=1}^{M} \frac{Z_k}{|\mathbf{r} - R_k|}. \tag{5}$$

The second term is the Hartree potential describing the interacting potential among the electrons, which can be written as

$$V_{Hartree}([\rho]; \mathbf{r}) = \int \frac{\rho(\mathbf{r}')}{|\mathbf{r} - \mathbf{r}'|} d\mathbf{r}'. \tag{6}$$

And the last term V_{xc} stands for the exchange-correlation potential, which is caused by the Pauli exclusion principle and other non-classical Coulomb interactions. The analytical expression for the exchange-correlation term is unknown. In this paper, we use Local Density Approximation (LDA) to generate the exchange-correlation potential [33].

Owing to the exponential decay behavior of the ground state wavefunction of the Schrödinger equation [1,41] , the current computational domain can be reasonably set by a bounded polyhedral domain $\Omega \subset \mathcal{R}^3$ in practical computations. Then the variational form of the Kohn–Sham equation on Ω can be formulated as: find $(\epsilon_i, \psi_i) \in \mathcal{R} \times H_0^1(\Omega)$, $i = 1, 2, \ldots, N$, such that

$$\int_\Omega \left\{ \frac{1}{2} \nabla\psi_i \nabla\varphi + V_{eff}\psi_i\varphi \right\} d\mathbf{r} = \epsilon_i \int_\Omega \psi_i \varphi d\mathbf{r}, \quad \forall \varphi \in H_0^1(\Omega), \tag{7}$$

where $H^1(\Omega)$ is the standard Sobolev space, $H_0^1(\Omega) = \{\varphi \in H^1(\Omega) : \varphi = 0 \text{ on } \partial\Omega\}$.

For simplicity, hereafter we denote the Hartree potential $V_{Hartree}$ as ϕ and the set of wavefunction $\{\psi_i\}$ as ψ. Thus the ground state energy can be represented in terms of ψ and ϕ

$$E(\psi, \phi) = \frac{1}{2} \sum_{i=1}^{N} \int_\Omega |\nabla\psi_i|^2 d\mathbf{r} + \int_\Omega \varepsilon_{xc}(\rho(\psi)) d\mathbf{r} - \int_\Omega \sum_{k=1}^{M} \frac{Z_k \rho(\psi)}{|\mathbf{r} - \mathbf{R}_k|} d\mathbf{r} + E_{Hartree}, \tag{8}$$

where

$$\psi_i \in H_0^1(\Omega), \text{ and } E_{Hartree} = -\frac{1}{8\pi}\int_\Omega |\nabla\phi|^2 d\mathbf{r} + \int_\Omega \rho(\psi)\phi d\mathbf{r}, \tag{9}$$

and the Hartree potential ϕ can be obtained by solving the following Poisson equation

$$-\frac{1}{4\pi}\nabla^2\phi(\mathbf{r}) = \rho(\mathbf{r}), \tag{10}$$

with some proper boundary conditions. The finite element method is adopted to discretize the Kohn–Sham equation (2) and the Poisson equation (10). Assume that the finite element space $V_h \subset H_0^1(\Omega)$ is constructed on the bounded domain Ω partitioned by $\mathcal{T} = \{\mathcal{T}_K, K = 1, 2, 3, \ldots, N_{ele}\}$, where N_{ele} denotes the total number of elements of $\mathcal{T}$. Then the discretized variation form of (7) becomes: find $(\epsilon_i^h, \psi_i^h) \in \mathcal{R} \times V_h, i = 1, 2, \ldots, N$ such that

$$\sum_{\mathcal{T}_K}\int_{\mathcal{T}_K}\left\{\frac{1}{2}\nabla\psi_i^h \cdot \nabla\varphi + V_{eff}\psi_i^h\varphi\right\} d\mathbf{r} = \epsilon_i^h \sum_{\mathcal{T}_K}\int_{\mathcal{T}_K}\psi_i^h\varphi d\mathbf{r}, \quad \forall\varphi \in V_h. \tag{11}$$

The k-th wavefunction ψ_k in the finite element space V_h can be approximated by

$$\psi_k^h = \sum_{i=1}^{N_{bas}} \psi_{k,i}^h \varphi_i, \tag{12}$$

where $\{\varphi_i\}, i = 1, \ldots, N_{bas}$ is the set of basis functions, N_{bas} denotes the dimension of the V_h. To find out $\Psi = \{\psi_{k,i}^h\}$, $i = 1, \ldots, N_{bas}$, i.e., the coefficients, we need to solve the variational form of the eigenvalue problem

$$A\Psi = \epsilon B\Psi, \tag{13}$$

where B is positive-definite and A and B are both Hermitian matrices. The entries of A, B are defined as

$$A_{ij} = \frac{1}{2}\int_\Omega \nabla\varphi_i \cdot \nabla\varphi_j d\mathbf{r} + \int_\Omega V_{eff}\varphi_i\varphi_j d\mathbf{r}, \tag{14}$$

$$B_{ij} = \int_\Omega \varphi_i\varphi_j d\mathbf{r}, \tag{15}$$

respectively.

Similarly, the Hartree potential ϕ_h in space V_h can be represented as

$$\phi_h = \sum_{i=1}^{N_{bas}} \phi_{h,i}\varphi_i, \tag{16}$$

where $\{\phi_{h,i}\}$ are coefficients (the values of wavefunctions on the corresponding nodes).

Furthermore, the Poisson equation (10) is discretized into the following form

$$P\phi_h = f, \tag{17}$$

with a Dirichlet boundary condition following the strategy in the paper [7], in which a multipole expansion approximation is adopted for the boundary values. Here P is a stiffness matrix with entry

$$p_{ij} = \int_\Omega \nabla\varphi_i \cdot \nabla\varphi_j d\mathbf{r}, \tag{18}$$

and f is a vector with entry

$$f_i = \int_\Omega 4\pi\rho(\mathbf{r})\varphi_i d\mathbf{r}. \tag{19}$$

3 *A posteriori* Error Estimate Based on an Asymptotic Analysis

In this section, we deliver *a posteriori* error estimate for Kohn–Sham equation. Some preliminary results are given firstly and then the *a posteriori* error estimate towards to the ground state energy is illustrated in this section.

3.1 Some Preliminary Results

The Hamiltonian operator H is given by

$$H = T + V_{ext} + \phi + V_{xc}. \tag{20}$$

The boundedness of the kinetic operator T in a bounded domain is obvious. In the following content in this subsection, we will first give some assumptions to show the boundedness of the exchange-correlation term following Chen et. al [13]. Then the boundedness of the external energy is proved by using the Hardy–type inequality [26]. Finally, the boundedness of the Hartree potential is discussed.

It is noted that $V_{xc} = d\varepsilon_{xc}/d\rho$, where ε_{xc} is the exchange-correlation energy per unit volume. The following assumptions [14] give the boundedness of V_{xc} directly

A_1 : $|\varepsilon'_{xc}(t)|+|t\varepsilon''_{xc}(t)|\in \mathscr{P}(p_1,(c_1,c_2))$ for some $p_1 \in [0,2]$, where $\mathscr{P}$ is a functional space defined as

$$\begin{aligned}&\mathscr{P}(p_1,(c_1,c_2))\\ &\quad=\{f : \exists\, a_1, a_2 \in \mathcal{R} \text{ such that } c_1 t^{p_1} + a_1 \le f(t) \le c_2 t^{p_1} + a_2, \forall t \ge 0\}.\end{aligned} \tag{21}$$

A_2 : There exists a constant $\alpha \in (0,1]$ such that

$$|\varepsilon''_{xc}(t)|+|t\varepsilon'''_{xc}(t)| \lesssim 1 + t^{\alpha-1} \quad \forall t > 0. \tag{22}$$

To deliver the boundedness of the external energy, we first introduce the Hardy–type inequality [26].

Theorem 1 *Let G be a Carnot group with homogeneous dimension $Q \ge 3$ and let $\phi \in C_0^\infty(G\backslash\{0\})$, $\alpha \in \mathcal{R}$, $Q+\alpha-2>0$. Then the following inequality is valid*

$$\int_G N^\alpha \mid \nabla_G \phi \mid^2 dx \ge \left(\frac{Q+\alpha-2}{2}\right)^2 \int_G N^\alpha \frac{\mid \nabla_G N \mid^2}{N^2}\phi^2 dx. \tag{23}$$

In this paper, we focus on the term $\int_{\mathcal{R}^3} Z_k|\psi_i|^2/|\mathbf{r}-R_k|d\mathbf{r}$, with the corresponding external energy given in the following form

$$E_{ext} = -\sum_{k=1}^{M}\int_\Omega \frac{\Psi^* Z_k \Psi}{|\mathbf{r}-R_k|}d\mathbf{r}. \tag{24}$$

Based on the above consideration and Theorem 1, we derive the following inequality.

Corollary 1 *Let R_k is the location of the k-th nuclei with the nuclear charge Z_k, ψ_i is the i-th wavefunction, then there exists a constant c such that*

$$\int_{\mathcal{R}^3} \frac{Z_k}{|\mathbf{r}-R_k|}|\psi_i|^2 d\mathbf{r} \leq c \int_{\mathcal{R}^3} |\mathbf{r}-R_k||\nabla\psi_i|^2 d\mathbf{r}, \tag{25}$$

Proof In the abelian case, when $G = \mathcal{R}^n$ with the ordinary dilations, one has $\mathcal{G} = \mathcal{R}^n$ ($\mathcal{G}$ is the Lie algebra of G), so that $Q = n$. In the Theorem 1, N is the homogeneous norm, which is a continuous function from G to $[0, \infty)$, satisfies: $N = u^{1/(2-Q)}$, where u is the Folland's solution for the sub-Laplacian ΔG.

Since the problem is set up in the real case, there is no imaginary part, and sub-Laplacian is just the Laplacian. In this case, we take $G = \mathcal{R}^3$, $Q = 3$,$\alpha = 1$, $\beta = -1$, $u = (x)^{-1}$ (the x here will be substituted by $(\mathbf{r} - R_k)$ later for the V_{ext}). So $N = |u^{1/(2-Q)}| = |u^{-1}| = |x|$. Then the inequality becomes

$$\int_{\mathcal{R}^3} |x||\nabla\psi_i|^2 dx \geq \int_{\mathcal{R}^3} \frac{|\nabla|x||^2}{|x|}|\psi_i|^2 dx. \tag{26}$$

Let $\psi_i = N^{-1}\omega$, $\omega \in C_0^\infty(\mathcal{R}^3\backslash\{0\})$, such that

$$|\nabla(N^{-1}\omega)|^2 = N^{-4}|\nabla N|^2\omega^2 - 2N^{-3}\omega\nabla N\nabla\omega + N^{-2}|\nabla\omega|^2. \tag{27}$$

Multiplying (27) on both sides by N and taking the integration, we have

$$\begin{aligned}\int_{\mathcal{R}^3} N|\nabla\Psi_i|^2 dx &= \int_{\mathcal{R}^3} N^{-3}|\nabla N|^2\omega^2 dx - \int_{\mathcal{R}^3} \Delta(N^{-1})\omega^2 dx + \int_{\mathcal{R}^3} N^{-1}|\nabla\omega|^2 dx \\ &\geq \int_{\mathcal{R}^3} N^{-3}|\nabla N|^2\omega^2 dx - \int_{\mathcal{R}^3} \Delta(N^{-1})\omega^2 dx,\end{aligned} \tag{28}$$

due to

$$-\Delta(N^{-1}) = -\Delta(u) \Rightarrow \Delta(N^{-1}) = \Delta(u). \tag{29}$$

By plugging (29) into (28), we have

$$\int_{\mathcal{R}^3} N|\nabla\psi_i|^2 dx \geq \int_{\mathcal{R}^3} \frac{|\nabla N|^2}{N}|\psi_i|^2 dx - \int_{\mathcal{R}^3} \Delta u\omega^2 dx. \tag{30}$$

As $\Delta u = 0$, the inequality (30) can be addressed as

$$\int_{\mathcal{R}^3} N|\nabla\psi_i|^2 dx \geq \int_{\mathcal{R}^3} \frac{|\nabla N|^2}{N}|\psi_i|^2 dx. \tag{31}$$

By plugging x with $(\mathbf{r} - R_k)$, the inequality turns to be

$$\int_{\mathcal{R}^3} |\mathbf{r}-R_k||\nabla\psi_i|^2 d\mathbf{r} \geq \int_{\mathcal{R}^3} \frac{|\nabla|\mathbf{r}-R_k||^2}{|\mathbf{r}-R_k|}|\psi_i|^2 d\mathbf{r}. \tag{32}$$

So finally we obtain

$$\begin{aligned}\int_{\mathcal{R}^3} \frac{Z_k}{|\mathbf{r}-R_k|}|\psi_i|^2 d\mathbf{r} &\leq c \int_{\mathcal{R}^3} \frac{|\nabla|\mathbf{r}-R_k||^2}{|\mathbf{r}-R_k|}|\psi_i|^2 d\mathbf{r} \\ &\leq c \int_{\mathcal{R}^3} |\mathbf{r}-R_k||\nabla\psi_i|^2 d\mathbf{r}.\end{aligned} \tag{33}$$

Based on the Lemma 2.1 and Corollary 2.2 of [4], it is easy to see that the above inequality also holds for a bounded domain Ω. Then the boundedness of the external energy comes immediately. □

Finally, we turn to the boundedness of Hartree potential. The corresponding weak form for Eq. (10) is defined as follows

$$\frac{1}{4\pi}a(\phi, v) = f(v), \tag{34}$$

where $a(\phi, v) = \int_\Omega \nabla\phi\nabla v d\mathbf{r}$, $f(v) = \int_\Omega \rho v d\mathbf{r}$, $v \in H_0^1(\Omega)$.

The boundedness of ϕ can be discussed as follows. Firstly, we use the V-elliptic property of the bilinear functional $a(\cdot, \cdot)$. There exists $\alpha > 0$ such that $\forall v \in V$,

$$a(v, v) \geq \alpha\|v\|^2. \tag{35}$$

By substituting v with ϕ in (35), we have

$$\frac{\alpha}{4\pi}\|\phi\|^2 \leq \frac{1}{4\pi}a(\phi, \phi) = f(\phi) \leq \|f\|^*\|\phi\|, \tag{36}$$

that is

$$\frac{\alpha}{4\pi}\|\phi\| \leq \|f\|^*. \tag{37}$$

Then by the definition of $\|f\|^*$ and Cauchy–Schwartz inequality, we can obtain the following result

$$\|f\|^* = \sup_{v\in V}\frac{\int_\Omega \rho v d\mathbf{r}}{\|v\|} \leq c\frac{\|\rho\|_{L_2}\|v\|_{L_2}}{\|v\|_{L_2}} = c\|\rho\|_{L_2}. \tag{38}$$

Since $\|\rho\|_{L_2}$ is bounded in Ω, we have that the term $\|f\|^*$ is bounded. Consequently, from the inequality (37), the boundedness of ϕ is proved.

3.2 *A Posteriori* Error Estimate

In this subsection, we derive *a posteriori* error indicator for total energy based on an asymptotic analysis. Consider that the numerical solutions can describe the behavior of the exact solution in the asymptotic region, it makes sense to generate the error indicator in the asymptotic region by using the difference between two numerical solutions obtained from mesh $\mathcal{T}^h$ and $\mathcal{T}^H$.

The energy functional for the Kohn–Sham equation is defined as

$$E(\psi, \phi) = \frac{1}{2}\sum_{i=1}^{N}\int_\Omega |\nabla\psi_i|^2 d\mathbf{r} + \int_\Omega \varepsilon_{xc}(\rho(\psi))d\mathbf{r} - \int_\Omega \sum_{k=1}^{M}\frac{Z_k\rho(\psi)}{|\mathbf{r} - R_k|}d\mathbf{r} + E_{Hartree}, \tag{39}$$

where $E_{Hartree} = -\frac{1}{8\pi}\int_\Omega |\nabla\phi|^2 d\mathbf{r} + \int_\Omega \rho(\psi)\phi d\mathbf{r}$.

The discretization form for total energy in the finite element space V_h with the mesh $\mathcal{T}^h$ is given by

$$\begin{aligned} E^h(\psi^h, \phi^h) =& \frac{1}{2}\sum_{i=1}^{N}\int_\Omega |\nabla\psi_i^h|^2 d\mathbf{r} + \int_\Omega \varepsilon_{xc}(\rho(\psi^h))d\mathbf{r} - \int_\Omega \sum_{k=1}^{M}\frac{Z_k\rho(\psi^h)}{|\mathbf{r} - R_k|}d\mathbf{r} \\ & - \frac{1}{8\pi}\int_\Omega |\nabla\phi^h|^2 d\mathbf{r} + \int_\Omega \rho(\psi^h)\phi^h d\mathbf{r}. \end{aligned} \tag{40}$$

Furthermore, we assume that the mesh $\mathcal{T}^H$ is obtained by globally coarsening the mesh $\mathcal{T}^h$ one time. Then the total energy of the system on the mesh $\mathcal{T}^H$ is given in a similar way with $(\tilde{\psi}^H, \tilde{\phi}^H)$ from the corresponding finite element space V_H, i.e.,

$$\begin{aligned} E^H(\tilde{\psi}^H, \tilde{\phi}^H) =& \frac{1}{2}\sum_{i=1}^{N}\int_\Omega |\nabla \tilde{\psi}_i^H|^2 d\mathbf{r} + \int_\Omega \varepsilon_{xc}(\rho(\tilde{\psi}^H))d\mathbf{r} - \int_\Omega \sum_{k=1}^{M}\frac{Z_k\rho(\tilde{\psi}^H)}{|\mathbf{r}-R_k|}d\mathbf{r} \\ & - \frac{1}{8\pi}\int_\Omega |\nabla\tilde{\phi}^H|^2 d\mathbf{r} + \int_\Omega \rho(\tilde{\psi}^H)\tilde{\phi}^H d\mathbf{r}. \end{aligned} \tag{41}$$

Next, we assume that ψ_H^h and ϕ_H^h are projections of eigenvectors ψ^h and Hartree potential ϕ^h from the space V_h onto the space V_H, respectively. It should be mentioned that we do not consider the difference of the eigenvalues between meshes in the following error estimation. By assuming that the numerical solutions $\tilde{\psi}^H, \tilde{\phi}^H$ are already in the asymptotic region of the exact solutions, we have

$$\begin{cases} \tilde{\psi}^H = \psi_H^h + \delta\psi^h, \\ \tilde{\phi}^H = \phi_H^h + \delta\phi^h, \end{cases} \tag{42}$$

with the perturbations $\delta\psi^h$ and $\delta\phi^h$.

So the total energy on the mesh $\mathcal{T}^H$ can be expanded as

$$\begin{aligned} E^H(\tilde{\psi}^H, \tilde{\phi}^H) =& E(\psi_H^h + \delta\psi^h, \phi_H^h + \delta\phi^h) = \frac{1}{2}\sum_{i=1}^{N}\int_\Omega |\nabla(\psi_{H,i}^h + \delta\psi_i^h)|^2 d\mathbf{r} \\ & + \int_\Omega \varepsilon_{xc}(\rho(\psi_H^h + \delta\psi^h))d\mathbf{r} - \int_\Omega \sum_{i=1}^{M}\frac{Z_k\rho(\psi_H^h + \delta\psi^h)}{|\mathbf{r}-R_k|}d\mathbf{r} \\ & - \frac{1}{8\pi}\int_\Omega |\nabla(\phi_H^h + \delta\phi^h)|^2 d\mathbf{r} + \int_\Omega \rho(\psi_H^h + \delta\psi^h)(\phi_H^h + \delta\phi^h)d\mathbf{r}. \end{aligned} \tag{43}$$

Using Taylor expansion, we can rewrite $E^H(\tilde{\psi}^H, \tilde{\phi}^H)$ in the following form

$$\begin{aligned} & E^H(\tilde{\psi}^H, \tilde{\phi}^H) \\ & = \frac{1}{2}\sum_{i=1}^{N}\int_\Omega (|\nabla\psi_{H,i}^h|^2 + |\nabla\delta\psi_i^h|^2 + 2\nabla\psi_{H,i}^h\nabla\delta\psi_i^h)d\mathbf{r} + \int_\Omega \varepsilon_{xc}(\rho(\psi_H^h))d\mathbf{r} \\ & \quad + 2\sum_{i=1}^{N}\int_\Omega \varepsilon'_{xc}(\rho(\psi_H^h))\psi_{H,i}^h\delta\psi_i^h d\mathbf{r} + 2\int_\Omega \varepsilon''_{xc}(\rho(\psi_H^h))\left(\sum_{i=1}^{N}\psi_{H,i}^h\delta\psi_i^h\right)^2 d\mathbf{r} \\ & \quad + \sum_{i=1}^{N}\int_\Omega \varepsilon'_{xc}(\rho(\psi_H^h))(\delta\psi_i^h)^2 d\mathbf{r} - \int_\Omega \sum_{i=1}^{N}\sum_{k=1}^{M}\frac{Z_k(|\psi_{H,i}^h|^2 + |\delta\psi_i^h|^2 + 2\psi_{H,i}^h\delta\psi_i^h)}{|\mathbf{r}-R_k|}d\mathbf{r} \\ & \quad - \frac{1}{8\pi}\int_\Omega (|\nabla\phi_H^h|^2 + |\nabla\delta\phi^h|^2 + 2\nabla\phi_H^h\nabla\delta\phi^h)d\mathbf{r} + \int_\Omega \rho(\psi_H^h)\phi_H^h d\mathbf{r} \\ & \quad + \int_\Omega \rho(\psi_H^h)\delta\phi^h d\mathbf{r} + 2\sum_{i=1}^{N}\int_\Omega \psi_{H,i}^h\delta\psi_i^h\phi_H^h d\mathbf{r} + 2\sum_{i=1}^{N}\int_\Omega \psi_{H,i}^h\delta\psi_i^h\delta\phi^h d\mathbf{r} \\ & \quad + \sum_{i=1}^{N}\int_\Omega (\delta\psi_i^h)^2\phi_H^h d\mathbf{r} + O((\delta\psi_i^h)^3, (\delta\psi_i^h)^2\delta\phi^h). \end{aligned} \tag{44}$$

Recalling that we want to propose an error indicator to the total energy directly, so in the remaining part of this section, we consider the error for the energy E which is given in the discretized form

$$\begin{aligned}
&E^H - E^h \\
&= \frac{1}{2}\sum_{i=1}^{N}\int_\Omega (|\nabla\delta\psi_i^h|^2 + 2\nabla\psi_{H,i}^h\nabla\delta\psi_i^h)d\mathbf{r} + 2\sum_{i=1}^{N}\int_\Omega \varepsilon'_{xc}(\rho(\psi_H^h))\psi_{H,i}^h\delta\psi_i^h d\mathbf{r} \\
&+ 2\int_\Omega \varepsilon''_{xc}(\rho(\psi_H^h))\left(\sum_{i=1}^{N}\psi_{H,i}^h\delta\psi_i^h\right)^2 d\mathbf{r} + \sum_{i=1}^{N}\int_\Omega \varepsilon'_{xc}(\rho(\psi_H^h))(\delta\psi_i^h)^2 d\mathbf{r} \\
&- \int_\Omega \sum_{i=1}^{N}\sum_{k=1}^{M}\frac{Z_k(|\delta\psi_i^h|^2 + 2\psi_{H,i}^h\delta\psi_i^h)}{|\mathbf{r}-R_k|}d\mathbf{r} - \frac{1}{4\pi}\int_\Omega \nabla\phi_H^h\nabla\delta\phi^h d\mathbf{r} \\
&- \frac{1}{8\pi}\int_\Omega |\nabla\delta\phi^h|^2 d\mathbf{r} + 2\sum_{i=1}^{N}\int_\Omega \psi_{H,i}^h\delta\psi_i^h\delta\phi^h d\mathbf{r} + \sum_{i=1}^{N}\int_\Omega (\delta\psi_i^h)^2\phi^h d\mathbf{r} \\
&+ 2\sum_{i=1}^{N}\int_\Omega \psi_{H,i}^h\delta\psi_i^h\phi_H^h d\mathbf{r} + \int_\Omega \rho(\psi_H^h)\delta\phi^h d\mathbf{r} + O((\delta\psi_i^h)^3, (\delta\psi_i^h)^2\delta\phi^h).
\end{aligned} \tag{45}$$

Now we turn to simplify (45) before estimating the error. It is noted that the orthonormality constraint functional is defined as

$$c(\psi_H^h) = \int_\Omega \psi_{H,i}^h\psi_{H,j}^h - \delta_{ij} = 0, \tag{46}$$

then we consider this functional for $\tilde{\psi}^H$,

$$\begin{aligned}
c(\tilde{\psi}^H) &= c(\psi_H^h + \delta\psi^h) \\
&= \int_\Omega (\psi_{H,i}^h + \delta\psi_i^h)(\psi_{H,j}^h + \delta\psi_j^h) - \delta_{ij} \\
&= \int_\Omega (\psi_{H,i}^h\psi_{H,j}^h + \psi_{H,i}^h\delta\psi_j^h + \delta\psi_i^h\psi_{H,j}^h + \delta\psi_i^h\delta\psi_j^h)d\mathbf{r} - \delta_{ij}.
\end{aligned}$$

Owing to

$$\int_\Omega \psi_{H,i}^h\psi_{H,j}^h = \delta_{ij}, \qquad c(\tilde{\psi}^H) = 0, \tag{47}$$

we can get

$$2\int_\Omega \psi_{H,i}^h\delta\psi_i^h d\mathbf{r} = -\int_\Omega (\delta\psi_i^h)^2 d\mathbf{r}.$$

That is,

$$2\sum_{i=1}^{N}\int_\Omega \epsilon_i\psi_i^h\delta\psi_i^h d\mathbf{r} = -\sum_{i=1}^{N}\int_\Omega \epsilon_i(\delta\psi_i^h)^2 d\mathbf{r}. \tag{48}$$

Meanwhile, the variational form of the model yield

$$\begin{cases} \frac{1}{2}\int_\Omega \nabla\psi^h_{H,i}\nabla\delta\psi^h_{H,i}d\mathbf{r} + \int_\Omega \varepsilon'_{xc}\psi^h_{H,i}\delta\psi^h_i d\mathbf{r} + \int_\Omega \phi^h_H\psi^h_{H,i}\delta\psi^h_i d\mathbf{r} \\ \quad -\int_\Omega \sum_{k=1}^{M}\frac{Z_k\psi^h_{H,i}\delta\psi^h_i}{|\mathbf{r}-R_k|}d\mathbf{r} = \int_\Omega \epsilon_i\psi^h_{H,i}\delta\psi^h_i d\mathbf{r}, \\ -\frac{1}{4\pi}\int_\Omega \nabla\phi^h_H\nabla\delta\phi^h d\mathbf{r} + \int_\Omega \rho(\psi^h_H)\delta\phi^h d\mathbf{r} = 0. \end{cases} \tag{49}$$

After plugging this into (45), we get the following error form for the energy E

$$\begin{aligned} &E^H - E^h \\ &= \frac{1}{2}\sum_{i=1}^{N}\int_\Omega |\nabla\delta\psi^h_i|^2 d\mathbf{r} - 2\sum_{i=1}^{N}\int_\Omega \epsilon_i(\delta\psi^h_i)^2 d\mathbf{r} \\ &\quad + 2\int_\Omega \varepsilon''_{xc}(\rho(\psi^h_H))\left(\sum_{i=1}^{N}\psi^h_{H,i}\delta\psi^h_i\right)^2 d\mathbf{r} \\ &\quad + \sum_{i=1}^{N}\int_\Omega \varepsilon'_{xc}(\rho(\psi^h_H))(\delta\psi^h_i)^2 d\mathbf{r} - \sum_{i=1}^{N}\int_\Omega\sum_{k=1}^{M}\frac{Z_k|\delta\psi^h_i|^2}{|\mathbf{r}-R_k|}d\mathbf{r} - \frac{1}{8\pi}\int_\Omega |\nabla\delta\phi^h|^2 d\mathbf{r} \\ &\quad + 2\sum_{i=1}^{N}\int_\Omega \psi^h_{H,i}\delta\psi^h_i\delta\phi^h d\mathbf{r} + \sum_{i=1}^{N}\int_\Omega (\delta\psi^h_i)^2\phi^h_H d\mathbf{r} + O((\delta\psi^h_i)^3, (\delta\psi^h_i)^2\delta\phi^h). \end{aligned} \tag{50}$$

Summing up the above, we reach the following result

$$\begin{aligned} &|E^H - E^h| \\ &\le \frac{1}{2}\sum_{i=1}^{N}\int_\Omega \left(|\nabla\delta\psi^h_i|^2 d\mathbf{r} + \left|\sum_{i=1}^{N}\int_\Omega \epsilon_i(\delta\psi^h_i)^2 d\mathbf{r}\right|\right) \\ &\quad + 2\left|\int_\Omega \varepsilon''_{xc}(\rho(\psi^h_H))\left(\sum_{i=1}^{N}\psi^h_{H,i}\delta\psi^h_i\right)^2 d\mathbf{r}\right| + \left|\sum_{i=1}^{N}\int_\Omega \varepsilon'_{xc}(\rho(\psi^h_H))(\delta\psi^h_i)^2 d\mathbf{r}\right| \\ &\quad + \sum_{i=1}^{N}\int_\Omega\sum_{k=1}^{M}\frac{Z_k|\delta\psi^h_i|^2}{|\mathbf{r}-R_k|}d\mathbf{r} + \frac{1}{8\pi}\int_\Omega |\nabla\delta\phi^h|^2 d\mathbf{r} \\ &\quad + 2\left|\sum_{i=1}^{N}\int_\Omega \psi^h_{H,i}\delta\psi^h_i\delta\phi^h d\mathbf{r}\right| + \left|\sum_{i=1}^{N}\int_\Omega (\delta\psi^h_i)^2\phi^h_H d\mathbf{r}\right|. \end{aligned} \tag{51}$$

Now, we estimate the error of (51) term by term. For the first term, using the definition of the semi-norm [15], it becomes

$$\begin{aligned} \sum_{i=1}^{N}\frac{1}{2}\int_\Omega |\nabla\delta\psi^h_i|^2 d\mathbf{r} &= \sum_{i=1}^{N}\frac{1}{2}\int_\Omega |\nabla(\psi^h_{H,i} - \tilde{\psi}^H_i)|^2 d\mathbf{r} \\ &= \frac{1}{2}\sum_{i=1}^{N}|\psi^h_{H,i} - \tilde{\psi}^H_i|^2_{1,\Omega}. \end{aligned} \tag{52}$$

For the second term, we have

$$
\begin{aligned}
2\left|\sum_{i=1}^{N}\int_{\Omega}\epsilon_i(\delta\psi_i^h)^2d\mathbf{r}\right| &\le \sum_{i=1}^{N}\int_{\Omega}|\epsilon_i|(\delta\psi_i^h)^2d\mathbf{r} \\
&= \sum_{i=1}^{N}|\epsilon_i|\int_{\Omega}(\psi_{H,i}^h-\tilde{\psi}_i^H)^2d\mathbf{r} \\
&\le c_3\sum_{i=1}^{N}\|\psi_{H,i}^h-\tilde{\psi}_i^H\|_{0,\Omega}^2.
\end{aligned}
\tag{53}
$$

For the third and fourth terms, we have

$$
\sum_{i=1}^{N}\left|\int_{\Omega}\varepsilon_{xc}'(\rho(\psi_H^h))(\delta\psi_i^h)^2d\mathbf{r}\right| \le \sum_{i=1}^{N}\int_{\Omega}|\varepsilon_{xc}'(\rho(\psi_H^h))||(\delta\psi_i^h)^2|d\mathbf{r}, \tag{54}
$$

$$
\left|\int_{\Omega}\varepsilon_{xc}''(\rho(\psi_H^h))\left(\sum_{i=1}^{N}\psi_{H,i}^h\delta\psi_i^h\right)^2d\mathbf{r}\right| \le \sum_{i=1}^{N}\int_{\Omega}|\varepsilon_{xc}''(\rho(\psi_H^h))||\rho(\psi_H^h)||\delta\psi_i^h|^2d\mathbf{r}. \tag{55}
$$

By combining the above two inequalities, it can be derived that

$$
\begin{aligned}
&\sum_{i=1}^{N}\left|\int_{\Omega}\varepsilon_{xc}'(\rho(\psi_H^h))(\delta\psi_i^h)^2d\mathbf{r}\right| + \left|\int_{\Omega}\varepsilon_{xc}''(\rho(\psi_H^h))\left(\sum_{i=1}^{N}\psi_{H,i}^h\delta\psi_i^h\right)^2d\mathbf{r}\right| \\
&\le \sum_{i=1}^{N}\int_{\Omega}[|\varepsilon_{xc}'(\rho(\psi_H^h))|+|\varepsilon_{xc}''(\rho(\psi_H^h))||\rho(\psi_H^h)|]|\delta\psi_i^h|^2d\mathbf{r}.
\end{aligned}
\tag{56}
$$

Recalling the assumption A_1 of local density approximation (LDA) for the exchange-correlation term, we find

$$
|\varepsilon_{xc}'(t)|+|t\varepsilon_{xc}''(t)| \in \mathcal{P}(p_1,(c_1,c_2)) \quad for\ some\ p_1\in[0,2], \tag{57}
$$

i.e. $\exists\, a_1, a_2 \in \mathcal{R}$ such that,

$$
a_1+c_1t^{p_1} \le |\varepsilon_{xc}'(t)|+|t\varepsilon_{xc}''(t)| \le a_2+c_2t^{p_1}, \tag{58}
$$

for any $t\ge 0$, $c_1\in\mathcal{R}$, $c_2\in[0,\infty)$. So (56) can be expressed as

$$
\begin{aligned}
&\sum_{i=1}^{N}\int_{\Omega}[|\varepsilon_{xc}'(\rho(\psi_H^h))|+|\varepsilon_{xc}''(\rho(\psi_H^h))||\rho(\psi_H^h)|]|\delta\psi_i^h|^2d\mathbf{r} \\
&\le (a_2+c_2t^{p_1})\sum_{i=1}^{N}\int_{\Omega}|\psi_{H,i}^h-\tilde{\psi}_i^H|^2d\mathbf{r} \\
&= (a_2+c_2t^{p_1})\sum_{i=1}^{N}\|\psi_{H,i}^h-\tilde{\psi}_i^H\|_{0,\Omega}^2,
\end{aligned}
\tag{59}
$$

where $t=\rho(\psi_H^h)=\sum_{i=1}^{N}\|\psi_{H,i}^h\|^2$.

The way we deal with the 5-th term is to use the estimation for the external term in Corollary 1,

$$\begin{aligned}\sum_{i=1}^{N}\int_{\Omega}\sum_{k=1}^{M}\frac{Z_k|\delta\psi_i^h|^2}{|\mathbf{r}-R_k|}d\mathbf{r} &\le \tilde{c_5}\int_{\Omega}\sum_{i=1}^{N}\sum_{k=1}^{M}Z_k|\mathbf{r}-R_k||\nabla\delta\psi_i^h|^2d\mathbf{r}\\ &\le c_5\sum_{i=1}^{N}\int_{\Omega}\nabla(\psi_{H,i}^h-\tilde{\psi}_i^H)|^2d\mathbf{r}\\ &= c_5\sum_{i=1}^{N}|\psi_{H,i}^h-\tilde{\psi}_i^H|_{1,\Omega}^2.\end{aligned} \tag{60}$$

Due to $\tilde{\phi}^H=\phi_H^h+\delta\phi^h$, the 6-th term becomes

$$\begin{aligned}\frac{1}{8\pi}\int_{\Omega}|\nabla\delta\phi^h|^2d\mathbf{r} &= \frac{1}{8\pi}\int_{\Omega}|\nabla(\phi_H^h-\tilde{\phi}^H)|^2d\mathbf{r}\\ &= \frac{1}{8\pi}|\phi_H^h-\tilde{\phi}^H|_{1,\Omega}^2.\end{aligned} \tag{61}$$

Using Cauchy–Schwartz and Sobolev inequalities to solve the 7-th term, we can get

$$\begin{aligned}\sum_{i=1}^{N}\left|\int_{\Omega}\psi_{H,i}^h\delta\psi_i^h\delta\phi^h d\mathbf{r}\right| &\le \sum_{i=1}^{N}\int_{\Omega}|\psi_{H,i}^h\delta\psi_i^h\delta\phi^h|d\mathbf{r}\\ &\le \sum_{i=1}^{N}\|\psi_{H,i}^h\|_{0,6,\Omega}\|\tilde{\psi}_i^h-\psi_{H,i}^h\|_{0,\Omega}\|\tilde{\phi}^H-\phi_H^h\|_{0,3,\Omega}\\ &\le c_7\sum_{i=1}^{N}\|\tilde{\psi}_i^H-\psi_{H,i}^h\|_{0,\Omega}\|\tilde{\phi}^h-\phi_H^h\|_{1,\Omega}.\end{aligned} \tag{62}$$

As for the 8-th term, using Cauchy–Schwartz inequality, the term can be updated as

$$\begin{aligned}\sum_{i=1}^{N}\left|\int_{\Omega}(\delta\psi_i^h)^2\phi_H^h d\mathbf{r}\right| &\le \sum_{i=1}^{N}\int_{\Omega}|(\delta\psi_i^h)^2\phi_H^h|d\mathbf{r}\\ &= \sum_{i=1}^{N}\int_{\Omega}|(\tilde{\psi}_i^H-\psi_{H,i}^h)^2\phi_H^h|d\mathbf{r}\\ &\le \sum_{i=1}^{N}\|\phi_H^h\|_{0,\Omega}\|\tilde{\psi}_i^H-\psi_{H,i}^h\|_{0,\Omega}^2\\ &\le c_8\sum_{i=1}^{N}\|\tilde{\psi}_i^H-\psi_{H,i}^h\|_{0,\Omega}^2.\end{aligned} \tag{63}$$

Combing (52), (53) and (59)–(63) together, and applying the arithmetic-geometric mean inequality on (62), we finally arrive,

$$
\begin{aligned}
|E^H - E^h| \leq & \frac{1}{2}\sum_{i=1}^{N}|\psi_{H,i}^h - \tilde{\psi}_i^H|_{1,\Omega}^2 + c_3\sum_{i=1}^{N}\|\psi_{H,i}^h - \tilde{\psi}_i^H\|_{0,\Omega}^2 \\
& + (a_2 + c_2 t^{p_1})\sum_{i=1}^{N}\|\psi_{H,i}^h - \tilde{\psi}_i^H\|_{0,\Omega}^2 + c_5\sum_{i=1}^{N}|\psi_{H,i}^h - \tilde{\psi}_i^H|_{1,\Omega}^2 \\
& + \frac{1}{8\pi}|\phi_H^h - \tilde{\phi}^H|_{1,\Omega}^2 + c_7\left[\sum_{i=1}^{N}\|\tilde{\psi}_i^H - \psi_{H,i}^h\|_{0,\Omega}^2 + \sum_{i=1}^{N}\|\tilde{\phi}^H - \phi_H^h\|_{1,\Omega}^2\right] \\
& + c_8\sum_{i=1}^{N}\|\tilde{\psi}_i^H - \psi_{H,i}^h\|_{0,\Omega}^2.
\end{aligned} \tag{64}
$$

Based on the triangle inequality $|E^H - E| \leq |E^H - E^h| + |E^h - E|$, and convergence orders are $O((2h_K)^{2k})$, $O((h_K)^{2k})$ for $|E^H - E^h|$ and $|E^h - E|$, respectively, it comes

$$
\begin{aligned}
|E^H - E| &\leq |E^H - E^h| + |E^h - E| \\
&\leq C\sum_{\mathcal{T}_k^H}\left(\sum_{i=1}^{N}\|\psi_{H,i}^h - \tilde{\psi}_i^H\|_{1,\mathcal{T}_k^H}^2 + \frac{1}{8\pi}|\phi_H^h - \tilde{\phi}^H|_{1,\mathcal{T}_k^H}^2 + \|\tilde{\phi}^H - \phi_H^h\|_{1,\mathcal{T}_k^H}^2\right),
\end{aligned} \tag{65}
$$

asymptotically $h \to 0$.

Till now, we get the *a posteriori* error indicator for the numerical solutions in V_H on the mesh $\mathcal{T}^H$. It is worth noting that in simulations, this error indicator will not be used to guide the mesh adaption for the coarsened mesh $\mathcal{T}^H$, instead it is used to refine the current mesh $\mathcal{T}^h$. We do this based on the considerations of efficiency and the assumption that the numerical solutions on $\mathcal{T}^H$ are in the asymptotic region of the real solutions such that the error indicator can describe the shape of the error on the computation domain. Usually, the *a posteriori* error estimate is designed for wave functions, while noting that our ultimate purpose is to reduce the error of the total energy in order to find a good approximation for the ground state energy. Therefore, in this paper we present an *a posteriori* error estimate towards to energy directly.

Based on the above analysis, the error indicator is obtained

$$
\eta_{loc} = \sum_{i=1}^{N}\|\psi_i^h - \tilde{\psi}_{h,i}^H\|_{1,\mathcal{T}_k^h}^2 + \|\tilde{\phi}_h^H - \phi^h\|_{1,\mathcal{T}_k^h}^2 + \frac{1}{8\pi}|\phi^h - \tilde{\phi}_h^H|_{1,\mathcal{T}_k^h}^2, \tag{66}
$$

where $\tilde{\psi}_{h,i}^H$ and $\tilde{\phi}_h^H$ represent the interpolations of the i-th wavefunction $\tilde{\psi}_i^H$ and the Hartree potential $\tilde{\phi}^H$ to the current mesh, respectively. It is obvious that η_{loc} is a local error indicator. We use η_{loc} on the mesh $\mathcal{T}^h$ to conduct the refinement of the mesh grids. After that, we get the new mesh $\mathcal{T}^{h_1}$. By globally coarsening mesh $\mathcal{T}^{h_1}$ for once, we can get the mesh $\mathcal{T}^{H_1}$, on which we can generate a new error indicator.

Remark 1 To give a glance on the comparison of three contributions in the error indicator (66), we list the following table to show the averaged value for each part in the error indicator in one step of the simulation of example LiH. It is should mentioned that although the error from the wavefunctions is dominant, the error from the Hartree potential is important on resolving the valence electrons in the simulations.

#Node	$\sum_i \|\psi_i^h - \tilde{\psi}_{h,i}^H\|_{1,\mathcal{T}_k^h}^2$	$\|\tilde{\phi}_h^H - \phi^h\|_{1,\mathcal{T}_k^h}^2$	$\frac{1}{8\pi}\|\phi^h - \tilde{\phi}_h^H\|_{1,\mathcal{T}_k^h}^2$
28,842	3.75e−2	4.19e−5	4.11e−7

Remark 2 From the theorems of Finite Element Method [15], we can get the following relations

$$\begin{aligned}\|\psi^h - \tilde{\psi}^H\|_{0,\Omega} &\le C \inf_{\varphi^H \in V_H} \|\psi^h - \varphi^H\|_{0,\Omega} \\ &\le C \left\| \psi^h - \prod_H \psi^h \right\|_{0,\Omega} \\ &\le C(2h)^{k+1} |\psi^h|_{k+1,\Omega} \\ &= C \sum_{\mathcal{T}_K^h} (2h_K)^{k+1} |\psi^h|_{k+1,\mathcal{T}_K^h},\end{aligned} \tag{67}$$

where the function $\psi^h \in H^{k+1}(\mathcal{T}_K^h) \cap V_h$.

Similarly, we can get the following results

$$\begin{aligned}\|\psi^h - \tilde{\psi}^H\|_{1,\Omega} &\le C \sum_{\mathcal{T}_K^h} (2h_K)^k |\psi^h|_{k+1,\mathcal{T}_K^h}, \\ |\psi^h - \tilde{\psi}^H|_{1,\Omega} &\le C \sum_{\mathcal{T}_K^h} (2h_K)^k |\psi^h|_{k+1,\mathcal{T}_K^h}, \\ \|\phi^h - \tilde{\psi}^H\|_{1,\Omega} &\le C \sum_{\mathcal{T}_K^h} (2h_K)^k |\phi^h|_{k+1,\mathcal{T}_K^h}, \\ |\phi^h - \tilde{\phi}^H|_{1,\Omega} &\le C \sum_{\mathcal{T}_K^h} (2h_K)^k |\phi^h|_{k+1,\mathcal{T}_K^h},\end{aligned} \tag{68}$$

where the function $\psi^h, \phi^h \in H^{k+1}(\mathcal{T}_K^h) \cap V_h$.

So, the error for the energy $|E^H - E^h|$ can be written as follows

$$|E^H - E^h| \le C \sum_{\mathcal{T}_K^h} (2h_K)^{2k} (|\psi^h|_{k+1,\mathcal{T}_K^h}^2 + |\phi^h|_{k+1,\mathcal{T}_K^h}^2 + (2h_K)^2 |\psi^h|_{k+1,\mathcal{T}_K^h}^2). \tag{69}$$

4 Algorithm

In this section, the framework depicted in the Algorithm 1 of the proposed numerical method is illustrated. In general, the method can be divided into two parts, namely, solution part and mesh adaption part. Particularly, the Kohn–Sham equation is first solved on the current mesh $\mathcal{T}^h$. Then the mesh adaption part will be implemented through a coarsening mesh skill. Precisely, the current mesh $\mathcal{T}^h$ is first globally coarsened for once to obtain the coarsened mesh $\mathcal{T}^H$. Then we solve the Kohn–Sham equation again on the coarsened mesh $\mathcal{T}^H$. Based on the presented *a posteriori* error estimation derived in the previous section, the error indicator for $\mathcal{T}^h$ is generated. Then a better mesh $\mathcal{T}_{new}^h$ is obtained through refining and/or coarsening $\mathcal{T}^h$ according to the interpolated error indicator. After the mesh adaption process,

the solution part is carried out on the refined mesh $\mathcal{T}_{new}^h$ and then the mesh adaption part will be adopted again. This is actually an iterative method, and the algorithm will be ended up once the convergence criterion is satisfied. We will demonstrate these two parts separately in the following contents.

Algorithm 1 Algorithm for obtaining the total ground state energy

Require: A finite element space V_h^0 on the initial mesh $\mathcal{T}_0$, and an initial guess for wavefuctions $\{\psi_i^0, i = 1, ..., N\}$.
1: Generate density from $\{\psi_i^0\}$.
2: SCF iterations to solve the Kohn–Sham equations in V_h^0 and then obtain the eigenpairs $\{\psi_i, \epsilon_i\}$ and the total ground state energy E_{tot}^{new}.
3: **while** $|E_{tot} - E_{tot}^{new}| > tol$ **do**
4: $E_{tot} = E_{tot}^{new}$.
5: Implement Algorithm Mesh adaption (Algorithm 3).
6: Update the wavefunctions, density and Hartree potential in the updated finite element space V_h^{new}.
7: SCF iterations to solve the Kohn–Sham equations in V_h^{new} and obtain the eigenpairs $\{\psi_i^{new}, \epsilon_i^{new}\}$ and the total ground state energy E_{tot}^{new}.
8: **end while**
9: Output the total energy E_{tot}^{new}.

4.1 Solution Part

In the Kohn–Sham equations, the Hamiltonian is determined by the density function $\rho(\mathbf{r})$. Particularly, the Hartree potential $V_{Hartree}$ and the exchange-correlation potential V_{xc} depend on the electron density. However, the electron density is obtained from the wavefunctions which can only be achieved by solving the Kohn–Sham equation. Accordingly, to solve the Kohn–Sham equation the self-consistent filed (SCF) methods have to be adopted. Indeed, in the mesh adaption part, we also have to solve the Kohn-Sham equation to get the solutions on the coarsened mesh. The solution part on a fixed current mesh is described in Algorithm 2.

Algorithm 2 Solution Part: SCF iteration to solve KS equations

Require: $TOL, MITER$
1: **while** $|E^{n+1} - E^n| > TOL$ or $iter < MITER$ **do**
2: Generate Hartree potential by solving the associated Poisson equation.
3: Discretize the eigenvalue problem $H\psi_i = \epsilon_i \psi_i$.
4: Solve the generalized eigenproblem, then $\{\psi_i\}$ and $\{\epsilon_i\}$ are obtained.
5: Update the density.
6: $iter++$
7: **end while**

To start the algorithm, an initial guess $\rho_0(\mathbf{r})$ for density should be given in the initial finite element space V_0 associated with the basis $\{\varphi_i\}$. With $\rho_0(\mathbf{r})$ we can obtain the Hatree potential $\phi(\mathbf{r})$ by solving the following Poisson equation

$$-\nabla^2\phi(\mathbf{r}) = 4\pi\rho_0(\mathbf{r}), \tag{70}$$

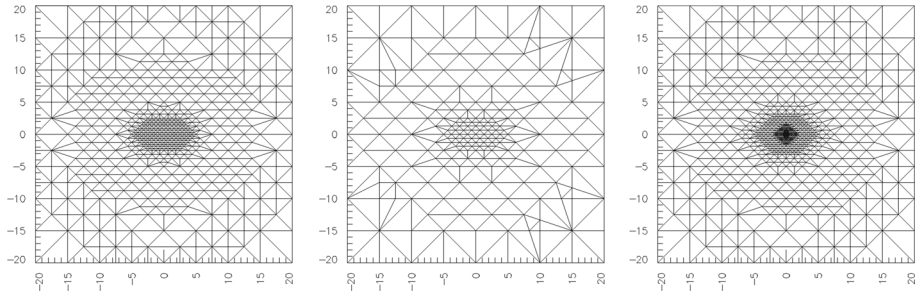

Fig. 1 One mesh adaption step in the simulation for the helium atom: the left mesh $\mathcal{T}^h$ is the initial mesh. Globally coarsening $\mathcal{T}^h$, we can get mesh $\mathcal{T}^H$ in the middle. Finally, after this mesh adaption process, the new mesh in the right $\tilde{\mathcal{T}}^h$ is obtained

with a proper Dirichlet boundary condition obtained following the strategy in the paper [7], in which a multipole expansion approximation is adopted for the boundary values. Meanwhile, the exchange-correction potential $V_{xc}(\mathbf{r})$ is obtained through the library Libxc [33]. As a result, the Hamiltonian is generated and then the Kohn–Sham equations are handled with the finite element discretization which results in the following eigenvalue problem

$$Ax = \lambda Mx, \tag{71}$$

where

$$A_{ij} = \langle \varphi_i | H \varphi_j \rangle, \qquad M_{ij} = \langle \varphi_i | \varphi_j \rangle.$$

To solve such an eigenvalue problem, the locally optimal block preconditioned conjugated gradient (LOBPCG) method [24,25] is used.

Once the eigenvalue problem is solved, the new electron density ρ is generated from the wavefuncitons and then the potentials $V_{Hartree}$ and V_{xc} are updated from the new density. The procedure will be repeated until the criterion for terminating the SCF iterations is satisfied. Subsequently, the mesh on the physical domain Ω is adaptively refined based on our mesh adaption method which will be described in detail in the next section. After the mesh adaption procedure, the finite element space V_h will be updated, and then the density function is interpolated from the old finite element space to the updated finite element space. With the interpolated density function, we solve the Kohn–Sham equation again and repeat the above process. As long as the difference of the densities between the two adjacent meshes is small enough, the program will be interrupted.

4.2 Mesh Adaption Part

In the mesh adaption procedure, an error indicator is generated from the comparisons between the information on the original mesh $\mathcal{T}^h$ and that on the coarsened mesh $\mathcal{T}^H$. Then the error indicator is used to indicate places to be refined or coarsened on $\mathcal{T}^h$. Figure 1 describes the variation of the mesh in one mesh adaption process during the simulation of helium atom. The workflow for mesh adaption procedure is demonstrated in Algorithm 3

Once the SCF iteration ends upon the mesh $\mathcal{T}^h$, $\mathcal{T}^h$ would be coarsened globally for once and from which we obtain $\mathcal{T}^H$. It is noted that in the practical simulations, the root elements may exist in $\mathcal{T}^h$ which results in that these elements will not be coarsened and finally kept in

Algorithm 3 Algorithm for mesh adaption

Require: A mesh $\mathcal{T}^h$ with wavefunctions $\{\psi_i^h\}$ on it.

1: Global coarsening the mesh for once, obtain $\mathcal{T}^H$.
2: Project ρ^h to ρ^H on $\mathcal{T}^H$.
3: SCF iteration on $\mathcal{T}^H$ to solve Kohn–Sham equations on $\mathcal{T}^H$, obtain $\{\tilde{\psi}_i^H\}$, $\{\tilde{\epsilon}_i^H\}$.
4: Generate the indicator η_{loc}^h on each element of $\mathcal{T}^h$ from Eq. (66).
5: Adaptively refine mesh $\mathcal{T}^h$.
6: Update the finite element space V_h and $\{\psi_i^h\}$ on the new mesh.

$\mathcal{T}^H$. Nevertheless, this phenomenon is acceptable since the error on these elements is already small enough and thus will not affect the accuracy of our algorithm.

The electron density ρ^h on mesh $\mathcal{T}^h$ is projected to ρ^H on $\mathcal{T}^H$. Then we will use the density ρ^H to generate the Hamiltonian on the coarse mesh. Note that, although the Hartree potential $V_{Hartree}^H$ on $\mathcal{T}^H$ is also obtained through solving the Poisson equation (70), we no longer need the multipole expansions to approximate the Dirichlet boundary condition. Alternately, the Hartree potential $\tilde{V}_{Hartree}^H$ on $\mathcal{T}^H$ which is the projection of $V_{Hartree}^h$ on mesh $\mathcal{T}^h$ will be used to generate the boundary condition for the Poisson equation (70). This makes sense since the Hartree potential on the mesh $\mathcal{T}^h$ is closer to the real Hartree potential than it on $\mathcal{T}^H$. The exchange-correlation is obtained immediately from the density ρ^H by the library Libxc.

After the evaluation of the Hamiltonian, the wavefuctions $\{\psi_i^h\}$ are first projected to the finite element space built on the coarse mesh $\mathcal{T}^H$. The projected wavefuncions $\{\psi_{H,i}^h\}$ are then set as the initial guess for the Kohn–Sham equation on mesh $\mathcal{T}^H$. Then the Kohn–Sham equation is solved and thus we get the wavefunctions $\{\tilde{\psi}_i^H\}$ and the Hartree potential $\tilde{\phi}^H$. To obtain the error indicator, $\{\tilde{\psi}_i^H\}$ and $\tilde{\phi}^H$ are thus interpolated back as $\{\tilde{\psi}_{h,i}^H\}$ and $\tilde{\phi}_h^H$ to the current mesh $\mathcal{T}^h$, respectively. Therefore, the error indicator is obtained from the Eq. (66). With this error indicator, the adaptive process is carried out on mesh $\mathcal{T}^h$. After mesh adaption, the electron density will be updated on the new mesh.

It is worth mentioning that the mesh adaption part only contributes a small part of the total computational cost. This can be explained in the following aspects: (1) the number of degree of freedoms on the coarsened mesh $\mathcal{T}^H$ is around 15% of the amount of the current mesh $\mathcal{T}^h$; (2) we have a qualified initial guess for the Kohn–Sham equation on the coarsened mesh which is the projection of the wavefuctions on the current mesh $\mathcal{T}^h$ to the coarsened mesh $\mathcal{T}^H$. As a result, the computational cost for the mesh adaption part only occupies a small proportion of that for the total algorithm, which is illustrated in Table 1 in the next section.

5 Numerical Examples

In this section, the convergence of the proposed method is examined first by the all-electron calculations of several atoms. Then the reliability of the method is demonstrated by the all-electron calculations of some molecules. Furthermore, the CPU time for the algorithm is considered and an improvement is given. All simulations are implemented by using a C++ library Adaptive Finite Element package for the AB-Initio Calculations (AFEABIC). In this library, the Libxc [33] is employed for the generation of the exchange-correlation potential and energy. The physical domain is set as $[-20, 20]^3$ a.u. in the simulations unless otherwise specified. The wavefunctions are initialized randomly on the finite element space established

on a uniform mesh of the physical domain. The tetrahedral elements are used in all the simulations. With the proposed method, the mesh will be refined adaptively.

5.1 Total Ground State Energy Simulations

5.1.1 Hydrogen

The governing equation for the hydrogen atom can be described as

$$\left[-\frac{1}{2}\nabla^2 + \frac{1}{r}\right]\psi(\mathbf{r}) = E\psi(\mathbf{r}). \tag{72}$$

This is a linear equation and the energy for the exact ground state is $E_{GS} = -0.5$ a.u.. To demonstrate the convergence order of our algorithm, both the linear finite element method and the quadratic finite element method are used to test this example. The numerical results are shown in Fig. 2. The numerical convergence order is showed to agree with the theoretical convergence order by linear finite element method ($O(h^2)$) and quadratic finite element method ($O(h^4)$). Moreover, the smaller the tolerance for the error indicator, the more accurate the solution is. This shows the reliability of the presented method. Besides, an interesting fact is observed that the convergence rate is increasing as the increase of the number of mesh grid. This fact is proved to be the result of mesh adaption process. As the mesh is refined on the regions with large error and coarsened on the regions with small error, a better result is obtained although the number of mesh grids increases little.

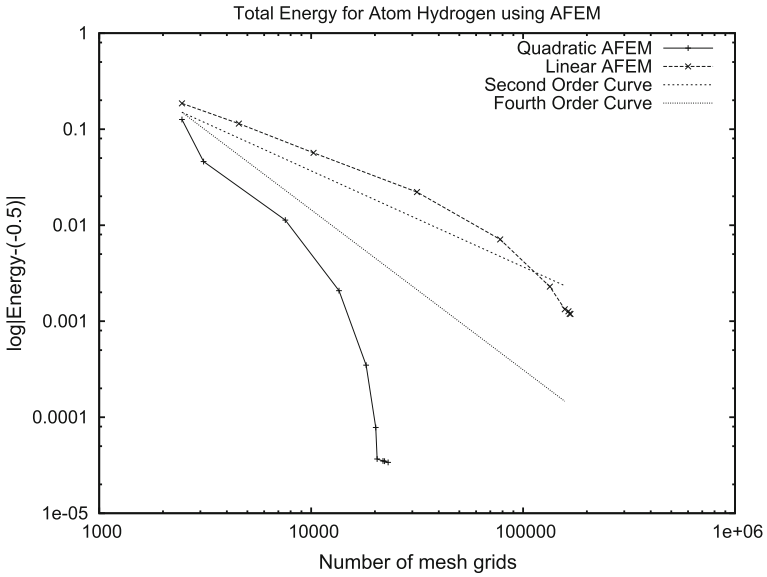

Fig. 2 Convergence rate of the ground state energy with linear AFEM and with quadratic AFEM for the hydrogen system

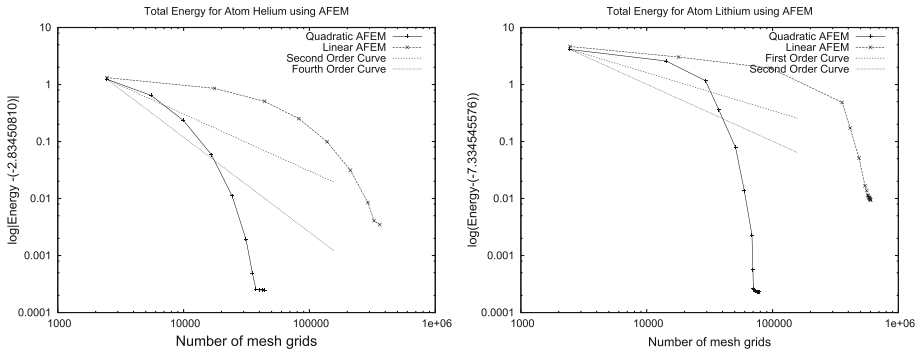

Fig. 3 Numerical results for Helium atom (left) and Lithium atom (right). Both linear and quadratic FEM are tested. The reference values for the total ground state energies are $E_{\mathrm{He}} = -2.83450810$ a.u., $E_{\mathrm{Li}} = -7.334545576$ a.u., respectively

5.1.2 Helium and Lithium

Following are the simulations for the Helium atom and lithium atom. Unlike the Hydrogen atom case, the governing equation becomes nonlinear and thus should be solved by SCF (self-consistent filed).

$$\left(-\frac{1}{2}\nabla^2 - \frac{Z}{r} + V_{Hartree} + V_{XC}\right)\psi_i = \epsilon_i \psi_i \tag{73}$$

where $Z = 2$ for Helium atom and $Z = 3$ for Lithium atom. On the one hand, compared to the linear finite element method, Fig. 3 shows that the quadratic adaptive finite element method converges faster. Besides, both the convergence order for Helium atom and Lithium atom meet the theoretical prediction. Since analytical solutions are not available for helium atom and lithium atom, the total ground state energies from a very fine mesh using quadratic finite element discretizations are used for references to calculate the approximation errors.

These simulations demonstrated that our method works well for the nonlinear and multi-electron orbital case.

5.1.3 Benzene

To illustrate the practical applicability of the proposed method, we test the total ground state energy for a benzene molecule (C_6C_6) with 42 electrons. The computational domain is set as $[-25, 25]^3$ a.u.. The convergence curve for the total energy is shown in the left of Fig. 4, from which we observe that the total energy converges to -230.623 a.u., which is very close to the referenced value -230.859 a.u. [22]. The isosurface for the density of the function is displayed in the right of Fig. 4.

5.2 The All-Electron Simulations of the Molecules: H_2 and LiH

The first simulation of the molecule contributes to the hydrogen molecule. From valence bond theory, there is only one bond in the molecule. To calculate its ground state, the all-electron calculation is implemented. The bond length of H_2 is set from 1 to 1.8 bohr. Note that the experimental value is 1.4011 bohr [22]. The numerical results are demonstrated in Fig. 5,

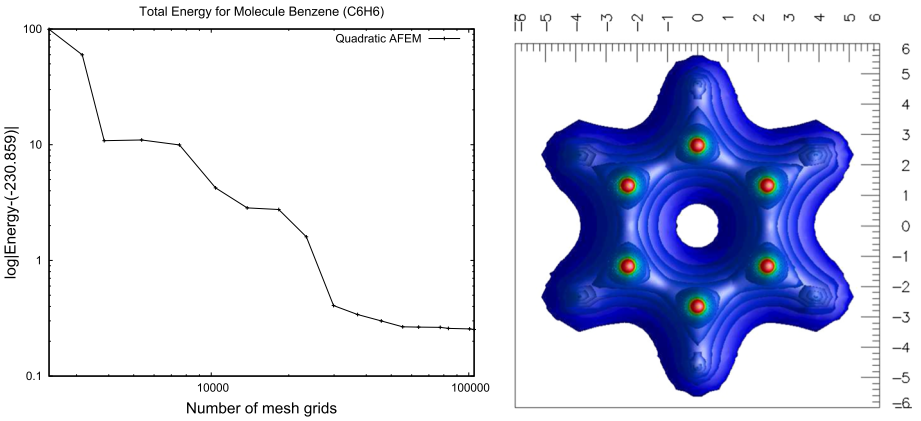

Fig. 4 Left: convergence curve for the energy of the molecule C_6C_6. Right: the density profile of C_6C_6

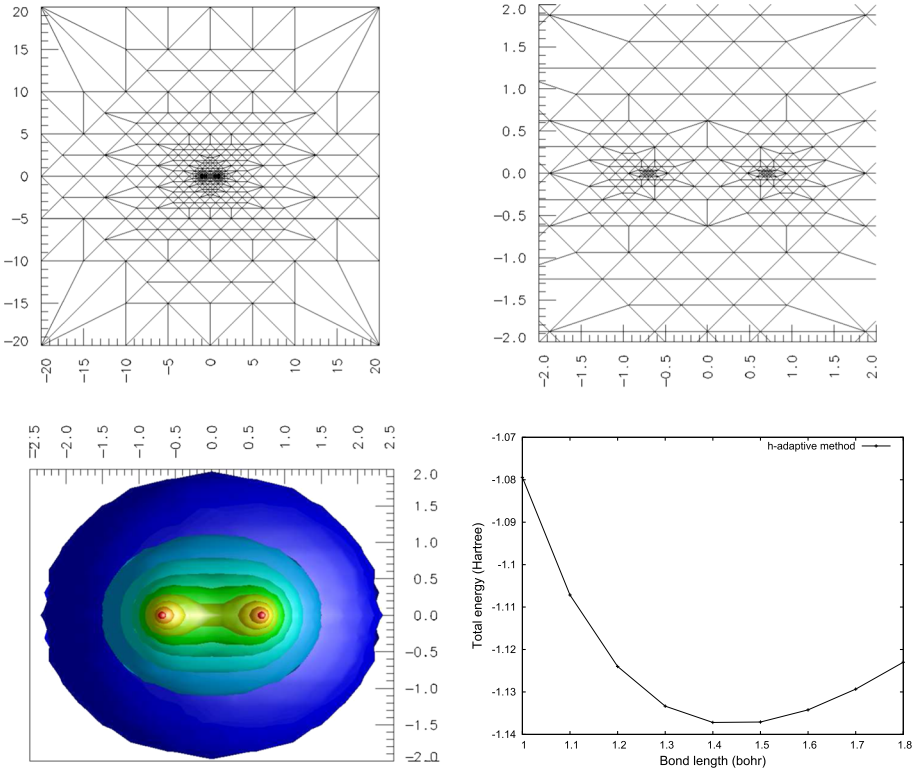

Fig. 5 The results for the H_2. Top left: the sliced mesh of the whole domain $[-20, 20]^3$ one the X-Y plane. Top right: the sliced mesh of the small domain $[-2, 2]^3$ on the X-Y plane. Bottom left: the density profile for the H_2 molecule. Bottom right: the relationship between total energy and H_2 bond length

and the following observations can be made from the results: (1) with our adaptive method, the regions with large variation of the electron density are successfully resolved by mesh grids, see Fig. 5 (top right). (2) It can be read from Fig. 5 (bottom right) that the optimal bond

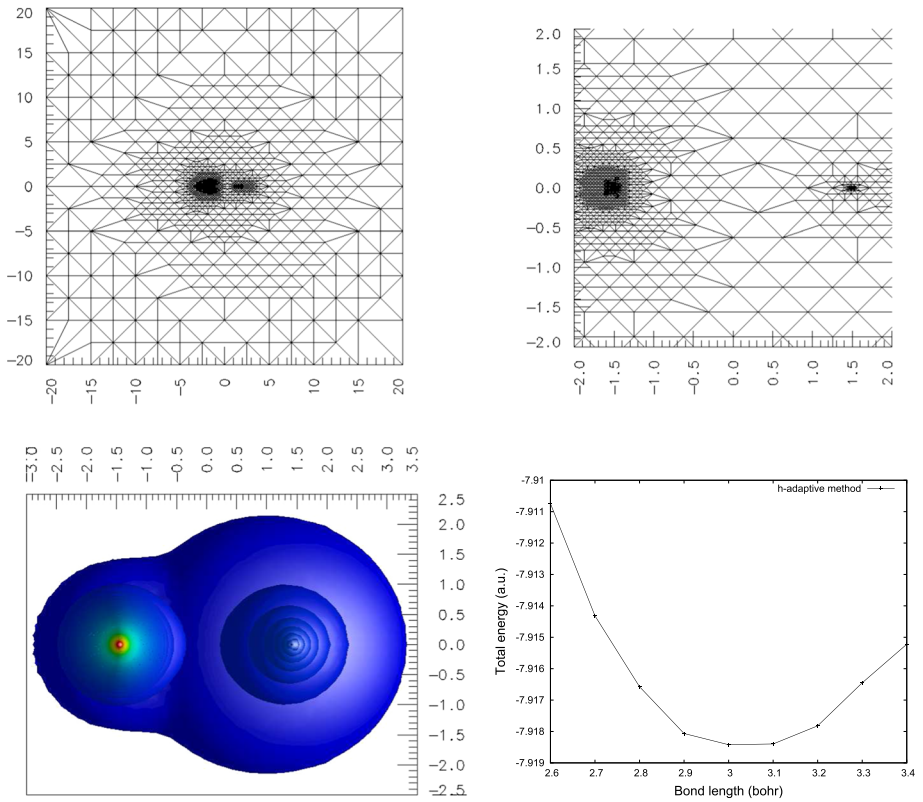

Fig. 6 The results for the LiH. Top left: the sliced mesh of the whole domain $[-20, 20]^3$ one the X-Y plane. Top right: the sliced mesh of the small domain $[-2, 2]^3$ on the X-Y plane. Bottom left: the density profile for the LiH molecule. Bottom right: the relationship between total energy and LiH bond length

length of H_2 from our calculation is around 1.4 bohr which is a good approximation to the experimental data.

Subsequently, we consider the all-electron calculation of the lithium hydride (LiH). The bond length of LiH is set from 2.6 to 3.4 bohr in the simulations. The numerical results are demonstrated in Fig. 6. Similar with the experiments of H_2 molecule, from Fig. 6 we can observe that the regions with large variation of density are resolved by mesh grids and that the optimal bond length in our calculation is around 3.0 bohr which agrees with the experiment data 3.014 [22]. Furthermore, since the all-electron calculation is adopted, it is expected that the electron density around the lithium nucleus is larger than that around the hydrogen nucleus which is obviously seen from Fig. 6 (bottom left). Moreover, from Fig. 6 (top right) the density of the mesh grids in the vicinity of the lithium nucleus is more intense than that around the hydrogen nucleus which shows that the variation of the electron density around the lithium nucleus is larger.

Remark 3 To better resolve the external potential, an auxiliary part

$$C \sum_{Nuc} \frac{1}{|\mathbf{r} - \mathbf{R}_{Nuc}|}$$

where C is a constant, is added to the error indicator. It is noted that the solutions to the Kohn–Sham equation are generally smooth, while the external potential terms are singular, which brings trouble in solving the equation. In the regions where the singularities located, the external potential is dominant in the Hamiltonian. Therefore, to describe the Hamiltonian better, the external potential should be carefully handled by the mesh. With the auxiliary part added to the error indicator, the mesh grids will be dense around the singular regions and the closer to the singularity, the denser the mesh grids. Furthermore, by controlling the value of the constant C, it is guaranteed that the error indicators at regions around the singularities will be affected only and that at other places will still be dominated by (66).

5.3 CPU Time Comparisons and an Improvement

The CPU time of the algorithm is studied in the simulation of the total energy for the ground state of a helium atom. In Fig. 7, the last dashed line describes the variation of the number of mesh grid in the simulation. From this figure, we can see that the most time-consuming part of the algorithm is the SCF iterations for solving the Kohn–Sham equation, including the solution on the current mesh and corresponding coarsened mesh. For the first five steps, the CPU time for SCF on current mesh and on coarsened mesh increase proportional to the number of the mesh grids. In this stage, the CPU time percentage for the SCF iteration on the coarsened mesh is around 12%, and that on the current mesh is around 88%. This data means that the mesh adaption procedure only attributes a small part to the computational cost of the total algorithm in the beginning. For the last five steps, we observe that the CPU time for the calculations on the current mesh decrease rapidly in spite of the increment of the number of mesh grids. However, the CPU time for the SCF iterations on the coarsened mesh changes

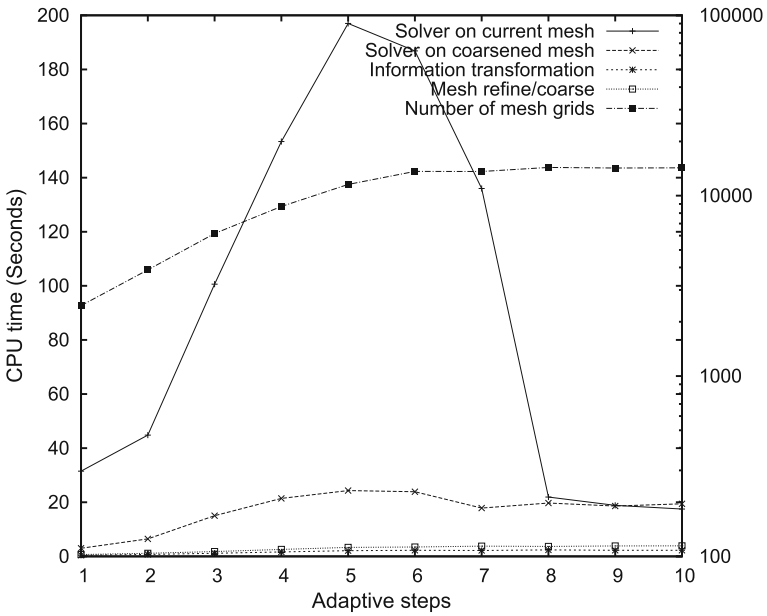

Fig. 7 The CPU time for each pact of the algorithm for solving the ground state of a helium atom. The eigensolver is used to solve the KS equation on the coarsened mesh

slightly, and as a result, the CPU time percentage for the mesh adaption part is increasing. This phenomenon can be explained: (1) it is noted that the number of mesh grids tends to be stable after the fifth adaptive step, which implies that the refined region of the mesh becomes small. Thus, the adjacent meshes are quite close. Consequently, the solutions on the two meshes are almost the same. As a result, the number of SCF iterations in each adaptive time step decreases to two even one since the initial guess is already near to the solution. So the CPU time for the SCF iterations on the current mesh decreases rapidly; (2) although the projected solution provides a good initial guess for the coarsened mesh, numerical results show that it still takes at least three iterations to resolve the compatible error generated from interpolation and projection. Therefore, the CPU cost of the mesh adaption part for the last several steps is almost unchanged. In total, the CPU time percentage for the mesh adaption procedure is about 15%, which is acceptable to us. However, the efficiency of the algorithm is still expected to be further improved.

To further improve the efficiency of our method, we try to find an alternative way to solve the Kohn–Sham equation in the coarsened mesh so that the amount of computational cost for mesh adaption procedure will decrease. Let us consider the Kohn–Sham equation

$$\left(-\frac{1}{2}\nabla^2 + V_{eff}\right)\psi = \epsilon\psi, \tag{74}$$

again. The corresponding variational form should be

$$\frac{1}{2}\int_\Omega \nabla\psi\nabla v d\mathbf{r} - \int_\Omega V_{eff}\psi v d\mathbf{r} = \epsilon\int_\Omega \psi v d\mathbf{r}, \quad \forall v \in V. \tag{75}$$

Now let us restrict the equation to the finite element space V_H built on mesh $\mathcal{T}^H$ and suppose (ϵ^H, ψ^H) be the projection of (ϵ, ψ) onto $\mathcal{T}^H$, which can represented as

$$\begin{cases} \epsilon = \epsilon^H + \delta\epsilon^H, \\ \psi = \psi^H + \delta\psi^H. \end{cases} \tag{76}$$

If we move the effective potential term together with the wavefunction $V_{eff}\psi$ to the right hand side, and then take the right hand side as the known source term, we obtain the following Poisson equation on the mesh $\mathcal{T}^H$

$$-\frac{1}{2}\nabla^2\tilde{\psi}^H = \epsilon\psi + V_{eff}\psi. \tag{77}$$

Plugging (76) in the Poisson equation, we get

$$\begin{aligned} -\frac{1}{2}\nabla^2\tilde{\psi}^H &= (\epsilon^H + \delta\epsilon^H)(\psi^H + \delta\psi^H) + V_{eff}(\psi^H + \delta\psi^H). \\ &= (\epsilon^H + V_{eff})\psi^H + O(\delta\psi^H, \delta\epsilon^H, \delta\psi^H\delta\epsilon^H), \end{aligned} \tag{78}$$

where $O(\delta\psi^H, \delta\epsilon^H, \delta\psi^H\delta\epsilon^H) = \epsilon^H\delta\psi^H + \delta\epsilon^H\psi^H + \delta\epsilon^H\delta\psi^H + V_{eff}\delta\psi^H$. Adding $\frac{1}{2}\nabla^2\psi^H$ to both sides of the above formula, we have

$$-\frac{1}{2}\nabla^2(\tilde{\psi}^H - \psi^H) = (\epsilon^H + V_{eff})\psi^H + \frac{1}{2}\nabla^2\psi^H + O(\delta\psi^H, \delta\epsilon^H, \delta\psi^H\delta\epsilon^H). \tag{79}$$

Then we multiply the formula (79) by $v \in V$, and apply integration by part, we can obtain

$$\begin{aligned}\frac{1}{2}\int_{\Omega}\nabla(\tilde{\psi}^H-\psi^H)\nabla v d\mathbf{r} &= \int_{\Omega}\epsilon^H\psi^H v d\mathbf{r}+\int_{\Omega}\left(-\frac{1}{2}\nabla\psi^H\nabla v+V_{eff}\psi^H v\right)d\mathbf{r}\\ &+\int_{\Omega}O(\delta\psi^H,\delta\epsilon^H,\delta\psi^H\delta\epsilon^H)v d\mathbf{r}.\end{aligned} \tag{80}$$

We define bilinear form

$$B(e,v)=\int_{\Omega}\epsilon^H\psi^H v d\mathbf{r}+\int_{\Omega}\left(-\frac{1}{2}\nabla\psi^H\nabla v+V_{eff}\psi^H v\right)d\mathbf{r}, \tag{81}$$

where e is residual of the wavefuction ψ^H for the Kohn–Sham equation on the space V_H.

Let us assume $\tilde{\Omega}_n$ be the support of the nodal function θ_n consisting of the patch of elements containing the vertex x_n ($\sum_{n\in\mathcal{N}}\theta_n(x)\equiv 1, x\in\bar{\Omega}$), and let $v=\tilde{\psi}^H-\psi^H$, then we have

$$\begin{aligned}&\left|\frac{1}{2}\int_{\tilde{\Omega}_n}\nabla(\tilde{\psi}^H-\psi^H)\nabla v d\mathbf{r}\right|\\ &=\left|-\frac{1}{2}\int_{\tilde{\Omega}_n}\nabla^2(\tilde{\psi}^H-\psi^H)d\mathbf{r}\right|\\ &=\left|\frac{1}{2}|\tilde{\psi}^H-\psi^H|^2_{2,\tilde{\Omega}_n}\right|\\ &=\left|B(e_n,\tilde{\psi}^H-\psi^H)+\int_{\tilde{\Omega}}O(\delta\psi^H,\delta\epsilon^H,\delta\psi^H\delta\epsilon^H)\delta\tilde{\psi}^H d\mathbf{r}\right|,\end{aligned} \tag{82}$$

where $e_n=e|_{\tilde{\Omega}}$. Moreover, if ψ^H stays in the asymptotic region of the KS equation, the integral term in the above formula can be neglected since it is a high order term. As a result,

$$\begin{aligned}&\left|\frac{1}{2}\int_{\tilde{\Omega}_n}\nabla(\tilde{\psi}^H-\psi^H)\nabla v d\mathbf{r}\right|\\ &=\left|B(e_n,\tilde{\psi}^H-\psi^H)+\int_{\tilde{\Omega}}O(\delta\psi^H,\delta\epsilon^H,\delta\psi^H\delta\epsilon^H)\delta\tilde{\psi}^H d\mathbf{r}\right|\\ &\le\tilde{C}\|e_n\|_{\tilde{\Omega}_n}\|\tilde{\psi}^H-\psi^H\|_{\tilde{\Omega}_n}\\ &\le C\||e_n|\|_{\tilde{\Omega}_n}|\tilde{\psi}^H-\psi^H|_{2,\tilde{\Omega}_n}.\end{aligned} \tag{83}$$

By defining the error estimator associated with the subdomain $\tilde{\Omega}$ as

$$\eta_n=\||e_n|\|_{\tilde{\Omega}_n}, \tag{84}$$

we can get the following relation using the subdomain residual method,

$$c_1\eta_n\le\|\psi-\psi^H\|\le c_2\eta_n, \tag{85}$$

where c_1, c_2 are constants.

Finally, we have the following theorem

Theorem 2 *If ψ^H stays in the asymptotic region of the Kohn–Sham equation, we have the following relationship between $\tilde{\psi}^H$ and ψ^H*

$$|\tilde{\psi}^H-\psi^H|_{2,\tilde{\Omega}_n}\le C\eta_n, \tag{86}$$

where C is a constant.

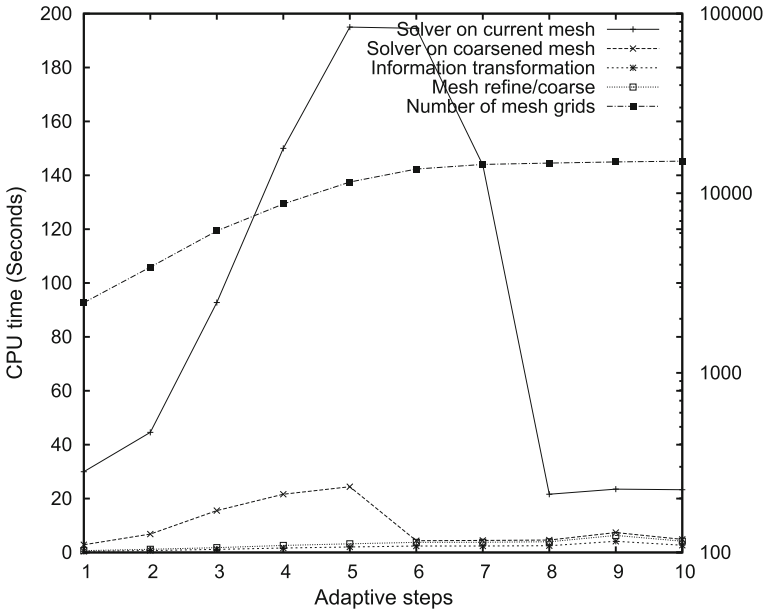

Fig. 8 The CPU time for each pact of the algorithm for solving the ground state of a helium atom. The solver on the coarsened mesh consists of two parts: the first five step we use an eigensolver, and for the remained steps we use the Poisson solver

Table 1 CPU time comparisons between solving KS equation on coarsened mesh and solving Poisson on coarsened mesh

Method	Energy	T_{tot}	T_{adapt}	$P_{adapt}(\%)$
KS-coarsening	−2.83346	1123.8	169.8	15.11
Poisson-coarsening	−2.83347	1067.6	97.0	9.09

Energy means the calculated ground state energy of the helium atom. T_{tot} stands for the CPU time of the whole algorithm, and T_{adapt} represents the CPU time for the mesh adaption part of the whole algorithm

From Theorem 2, we can conclude that the solution to the Poisson equation (79) can provide an effective approximation to the Kohn–Sham equation.

Based on above analysis, the solver for KS equation on the coarsened mesh is replaced from eigensolver to a Poisson solver after the fifth adaptive step. The CPU time for each part is displayed in Fig. 8 and the comparison between the original method and the new one is shown in Table 1. The reason why we do not use the Poisson solver from the beginning is that the Poisson solver generates an approximation only when the solution on the current mesh is good enough, i.e., the solution on the current mesh should stay in the asymptotic region of the KS equation. And this requirement will be satisfied if the number of mesh grids of the current mesh behaves stable. As displayed in Fig. 8 and Table 1, the number of mesh grids and the total ground state energy for the final mesh are almost the same with the former method, while the CPU time percentage decreases from 15.11 to 9.09%. On the other hand, we also can find that the total CPU time changes slightly. Nevertheless, it is expected that the lager the scale of the quantum system, the more the total CPU time decreases since more SCF iterations are needed for solution on the coarsened mesh. Therefore, according to this

consideration and these results, the Poisson solver which takes less computational cost can replace the eigensolver on the coarsened mesh for solving the KS equation.

6 Conclusions

In this paper, we developed an h-adaptive finite element method based on *a posteriori* error estimation to solve the Kohn–Sham equation. The SCF iteration is used for the nonlinear eigenvalue problem, and the LOBPCG method is adopted as the solver for the linear eigenvalue problem at each iteration. To improve the efficiency of the finite element solver, an h-adaptive method based *a posteriori* error estimation is introduced. The error indicator is generated from the difference between the solution information on the current finite element space and that on the finite element space built on the coarsened mesh. With such an error indicator, we refine or coarsen the current mesh to obtain a new mesh which can resolve the equations better.

Several numerical experiments including simulations of atoms and molecules have been conducted by using our method. The numerical results show that our solver is convergent and reliable. Specifically, we compare the linear finite element discretization and the quadratic finite element discretization in the simulations of atoms, and the results indicate that the convergence order of the method agree with expected. Moreover, during the calculation of the relationship between the bond length and the total ground state energy for the molecules, after the nuclei move, the distribution of the mesh grids can be improved accordingly with the presented h-adaptive method. That means the quality of the mesh grid is improved dynamically in our solver, which is more efficient than remeshing when a fixed mesh is no longer appropriate. To further improve the efficiency of our method, we solve the Poisson equation (77) instead of the Kohn–Sham equation in the coarsened mesh when the solution of the Kohn–Sham equation on the coarsened mesh has fall into the asymptotic region of the equation. The simulation shows that the new method takes less computational cost than the old one without loss of accuracy.

Acknowledgements This work was partially supported by FDCT 029/2016/A1 from Macao SAR, MYRG2017-00189-FST from University of Macau, and National Natural Science Foundation of China (Grant No. 11401608).

References

1. Agmon, S.: Lectures on Exponential Decay of Solutions of Second-Order Elliptic Equations: Bounds on Eigen functions of N-Body Schrodinger Operations (MN-29). Princeton University Press, Princeton (2014)
2. Ainsworth, M., Oden, J.T.: A Posteriori Error Estimation in Finite Element Analysis, vol. 37. Wiley, Hoboken (2011)
3. Akin, J., Singh, M.: Object-oriented Fortran 90 P-adaptive finite element method. Adv. Eng. Softw. **33**(7), 461–468 (2002)
4. Azorero, J.G., Alonso, I.P.: Hardy inequalities and some critical elliptic and parabolic problems. J. Differ. Equ. **144**(2), 441–476 (1998)
5. Bänsch, E., Siebert, K.G.: A Posteriori Error Estimation for Nonlinear Problems by Duality Techniques. Albert-Ludwigs-University, Math. Fak. (1995)
6. Bao, G., Hu, G., Liu, D.: An h-adaptive finite element solver for the calculations of the electronic structures. J. Comput. Phys. **231**(14), 4967–4979 (2012)
7. Bao, G., Hu, G., Liu, D.: Numerical solution of the Kohn–Sham equation by finite element methods with an adaptive mesh redistribution technique. J. Sci. Comput. **55**(2), 372–391 (2013)

8. Bao, G., Hu, G., Liu, D.: Towards translational invariance of total energy with finite element methods for Kohn–Sham equation. Commun. Comput. Phys. **19**(1), 1–23 (2016)
9. Becker, R., Rannacher, R.: An optimal control approach to a posteriori error estimation in finite element methods. Acta Numer. **10**, 1–102 (2001)
10. Belytschko, T., Tabbara, M.: H-Adaptive finite element methods for dynamic problems, with emphasis on localization. Int. J. Numer. Methods Eng. **36**(24), 4245–4265 (1993)
11. Castro, A., Appel, H., Oliveira, M., Rozzi, C.A., Andrade, X., Lorenzen, F., Marques, M.A., Gross, E., Rubio, A.: Octopus: a tool for the application of time-dependent density functional theory. Phys. Status Solidi (b) **243**(11), 2465–2488 (2006)
12. Chelikowsky, J.R., Troullier, N., Saad, Y.: Finite-difference-pseudopotential method: electronic structure calculations without a basis. Phys. Rev. Lett. **72**(8), 1240 (1994)
13. Chen, H., Dai, X., Gong, X., He, L., Zhou, A.: Adaptive finite element approximations for Kohn–Sham models. Multiscale Models Simul. **12**(4), 1828–1869 (2014)
14. Chen, H., Gong, X., He, L., Yang, Z., Zhou, A.: Numerical analysis of finite dimensional approximations of Kohn–Sham models. Adv. Comput. Math. **38**(2), 225–256 (2013)
15. Ciarlet, P.G.: The Finite Element Method for Elliptic Problems. SIAM, Philadelphia (2002)
16. Durán, R.G., Padra, C., Rodríguez, R.: A posteriori error estimates for the finite element approximation of eigenvalue problems. Math. Model. Methods Appl. Sci. **13**(08), 1219–1229 (2003)
17. Fiolhais, C., Nogueira, F., Marques, M.A.: A Primer in Density Functional Theory, vol. 620. Springer, Berlin (2003)
18. Gygi, F.: Electronic-structure calculations in adaptive coordinates. Phys. Rev. B **48**(16), 11692 (1993)
19. Gygi, F., Galli, G.: Real-space adaptive-coordinate electronic-structure calculations. Phys. Rev. B **52**(4), R2229 (1995)
20. Heuveline, V., Rannacher, R.: A posteriori error control for finite element approximations of elliptic eigenvalue problems. Adv. Comput. Math. **15**(1), 107–138 (2001)
21. Hu, G., Xie, H., Xu, F.: A multilevel correction adaptive finite element method for Kohn–Sham equation. J. Comput. Phys. **355**, 436–449 (2018)
22. Johnson III, R.D.: NIST Computational Chemistry Comparison and Benchmark Database. http://cccbdb.nist.gov/ (2016). Accessed 6 Oct 2018
23. Jiang, X., Zhang, L., Zheng, W.: Adaptive hp-finite element computations for time-harmonic Maxwell's equations. Commun. Comput. Phys. **13**(2), 559–582 (2013)
24. Knyazev, A.V.: Toward the optimal preconditioned eigensolver: locally optimal block preconditioned conjugate gradient method. SIAM J. Sci. Comput. **23**(2), 517–541 (2001)
25. Knyazev, A.V., Argentati, M.E., Lashuk, I., Ovtchinnikov, E.E.: Block locally optimal preconditioned eigenvalue xolvers (BLOPEX) in HYPRE and PETSc. SIAM J. Sci. Comput. **29**(5), 2224–2239 (2007)
26. Kombe, I.: Hardy, Rellich and uncertainty principle inequalities on Carnot groups. arXiv preprint arXiv:math/0611850 (2006)
27. Kormann, K.: A time-space adaptive method for the Schrödinger equation. Commun. Comput. Phys. **20**(1), 60–85 (2016)
28. Kresse, G., Furthmüller, J.: Efficient iterative schemes for ab initio total-energy calculations using a plane-wave basis set. Phys. Rev. B **54**(16), 11169 (1996)
29. Kuang, Y., Hu, G.: An adaptive FEM with ITP approach for steady Schrödinger equation. Int. J. Comput. Math. **95**(1), 187–201 (2018)
30. Larson, M.G.: A posteriori and a priori error analysis for finite element approximations of self-adjoint elliptic eigenvalue problems. SIAM J. Numer. Anal. **38**(2), 608–625 (2000)
31. Li, R., Tang, T., Zhang, P.: Moving mesh methods in multiple dimensions based on harmonic maps. J. Comput. Phys. **170**(2), 562–588 (2001)
32. Lin, L., Lu, J., Ying, L., Weinan, E.: Adaptive local basis set for Kohn–Sham density functional theory in a discontinuous Galerkin framework I: total energy calculation. J. Comput. Phys. **231**(4), 2140–2154 (2012)
33. Marques, M.A., Oliveira, M.J., Burnus, T.: Libxc: a library of exchange and correlation functionals for density functional theory. Comput. Phys. Commun. **183**(10), 2272–2281 (2012)
34. Motamarri, P., Nowak, M.R., Leiter, K., Knap, J., Gavini, V.: Higher-order adaptive finite-element methods for Kohn–Sham density functional theory. J. Comput. Phys. **253**, 308–343 (2013)
35. Pask, J., Sterne, P.: Finite element methods in ab initio electronic structure calculations. Model. Simul. Mater. Sci. Eng. **13**(3), R71 (2005)
36. Radovitzky, R., Ortiz, M.: Error estimation and adaptive meshing in strongly nonlinear dynamic problems. Comput. Methods Appl. Mech. Eng. **172**(1–4), 203–240 (1999)
37. Tsuchida, E., Tsukada, M.: Electronic-structure calculations based on the finite-element method. Phys. Rev. B **52**(8), 5573 (1995)

38. Verfürth, R.: A Review of a Posteriori Error Estimation and Adaptive Mesh-Refinement Techniques. Wiley, Hoboken (1996)
39. Xie, C., Hu, X.: Finite element simulations with adaptively moving mesh for the reaction diffusion system. Numer. Math. Theory Methods Appl. **9**(4), 686–704 (2016)
40. Yang, C., Meza, J.C., Lee, B., Wang, L.W.: KSSOLV-a MATLAB toolbox for solving the Kohn–Sham equations. ACM Trans. Math. Softw. (TOMS) **36**(2), 10 (2009)
41. Yserentant, H.: Regularity and Approximability of Electronic Wave Functions. Springer, Berlin (2010)
42. Zhang, G., Lin, L., Hu, W., Yang, C., Pask, J.E.: Adaptive local basis set for Kohn–Sham density functional theory in a discontinuous Galerkin framework II: force, vibration, and molecular dynamics calculations. J. Comput. Phys. **335**, 426–443 (2017)
43. Zhang, H., Zegeling, P.A.: A moving mesh finite difference method for non-monotone solutions of non-equilibrium equations in porous media. Commun. Comput. Phys. **22**(4), 935–964 (2017)